LITHOS 404-405 (2021) 106444

Contents lists available at ScienceDirect

LITHOS

journal homepage: www.elsevier.com/locate/lithos

Research Article

The origin of the earliest Jurassic basaltic rocks in southern Jiangxi Province, southeastern China: Implications for interaction between the asthenosphere and metasomatised lithosphere

Wei-Guang Zhu [a], Hong Zhong [a,b,*], Hui-Qing Huang [c], Zhong-Jie Bai [a], Yan-Jun Wang [d], Jun-Hua Yao [a], Peng-Cheng Hu [a]

[a] State Key Laboratory of Ore Deposit Geochemistry, Institute of Geochemistry, Chinese Academy of Sciences, 99 West Lincheng Road, Guiyang 550081, China
[b] University of Chinese Academy of Sciences, Beijing 100049, China
[c] Economic Geology Research Center, College of Science and Engineering, Division of Tropical Environments and Societies, James Cook University, Townsville, QLD 4811, Australia
[d] State Key Laboratory of Nuclear Resources and Environment, East China University of Technology, Nanchang 330013, China

ARTICLE INFO

Keywords:
Earliest Jurassic basalts
Geochemistry
Asthenosphere–lithosphere interactions
Continental extension
Southeastern China

ABSTRACT

Compositions of the earliest Jurassic basalts (190–188 Ma) from the the Baimianshi, Changpu, and Dongkeng basins in southern Jiangxi Province provide insight into the nature of their mantle sources as well as evidence for asthenosphere–lithospheric mantle interaction beneath Southeastern China. We report for the first time elemental and Sr—Nd isotopic data for the basalts collected from new drill cores. The basalts are mainly tholeiitic and subordinate alkaline basalts. The alkaline basalts have high TiO_2 contents (3.13–4.19 wt%), and high Ti/Y (596–699) and Nb/Y ratios (0.85–0.92) and Nb/La ratios (0.80–0.95). These basalts are characterised by ocean island basalt (OIB)-like trace element characteristics, and have primitive mantle-like $\varepsilon_{Nd}(t)$ values (−0.85 to +0.33) and moderately elevated $(^{87}Sr/^{86}Sr)_i$ ratios (0.7074–0.7082). The tholeiitic basalts have a large range of TiO_2 contents (1.26–3.26 wt%) and Nb/La ratios (0.40–0.88), plus relatively low Ti/Y (135–534) and Nb/Y ratios (0.32–0.69). Based on Nb/La ratios, the tholeiitic basaltic rocks can further divided into two sub-types: high Nb/La (Nb/La > 0.70) and low Nb/La (Nb/La < 0.70) tholeiitic basalts. The high Nb/La tholeiitic basalts exhibit slight Nb—Ta depletions (Nb/La = 0.73–0.88), mostly positive $\varepsilon_{Nd}(t)$ values (−0.04 to +2.5) and slightly elevated $(^{87}Sr/^{86}Sr)_i$ ratios (0.7061–0.7088), whereas the low Nb/La tholeiitic basalts exhibit moderate to large Nb—Ta depletions (Nb/La = 0.40–0.65), much lower $\varepsilon_{Nd}(t)$ values (−7.4 to −0.60) and higher $(^{87}Sr/^{86}Sr)_i$ ratios (0.7082–0.7115). In particular, the two low Nb/La tholeiitic basalts (termed as "high-Ba tholeiitic basalts" in this study) are characterised by island arc-like trace element features, such as significant enrichments in Ba and Th, and depletions in Nb, Ta, P, and Ti (Nb/La = 0.40). The two high-Ba basalts also exhibit significantly lower $\varepsilon_{Nd}(t)$ values (−7.3 to −7.4) and higher $(^{87}Sr/^{86}Sr)_i$ ratios (0.7112–0.7115). Based on the results, we propose that the parental magmas of the alkaline basalts were produced by low degrees (& 5%–7%) of partial melting of an asthenospheric mantle source at the depth within the garnet–spinel-bearing mantle with more garnet than spinel, the parental magmas of the high Nb/La tholeiitic basalts were generated by moderate degrees (& 15%–20%) of partial melting of a depleted asthenospheric mantle at a relatively shallow depth within the garnet–spinel stability field, the parental magmas of the high-Ba tholeiitic basalts were derived from lithospheric mantle that had been metasomatised by subducted sediment-derived melts and/or fluids. We envision the formation of tholeiitic to alkaline basaltic magmas in the earliest Jurassic in South China records was the result of interactions between the asthenosphere and metasomatised lithosphere during upwelling of the asthenospheric mantle that was triggered by the foundering and/or delamination of a subducted flat slab beneath this region and steep NW-ward palaeo-Pacific subduction.

* Corresponding author at: State Key Laboratory of Ore Deposit Geochemistry, Institute of Geochemistry, Chinese Academy of Sciences, 99 West Lincheng Road, Guiyang 550081, China.
E-mail address: zhonghong@vip.gyig.ac.cn (H. Zhong).

https://doi.org/10.1016/j.lithos.2021.106444
Received 17 April 2021; Received in revised form 29 August 2021; Accepted 30 August 2021
Available online 3 September 2021

1. Introduction

Compositions of continental basaltic rocks can be used to identify the nature of their mantle source(s), provide evidence for asthenosphere–lithosphere interactions, and constrain the regional tectonic evolution (Brown and White, 1995; Garfunkel, 2008; Hoernle et al., 2006; Saunders, 2005; Timm et al., 2009; White and McKenzie, 1989). Late Mesozoic igneous rocks, dominated by abundant granitoids and rhyolites with subordinate mafic igneous rocks, are widespread in southeastern China (Li et al., 2007a, 2007b; Zhou et al., 2006). Early Jurassic volcanic rocks (basalts and rhyolites), A-type granitoids, and minor syenites and gabbros occur mainly in the Nanling Range. In inland South China, the bimodal volcanic rocks occur in several small Early Jurassic basins. Early Jurassic basaltic rocks are volumetrically minor in South China, but their petrogenesis has significant implications for the tectonic evolution and formation of a coeval large granitic province in

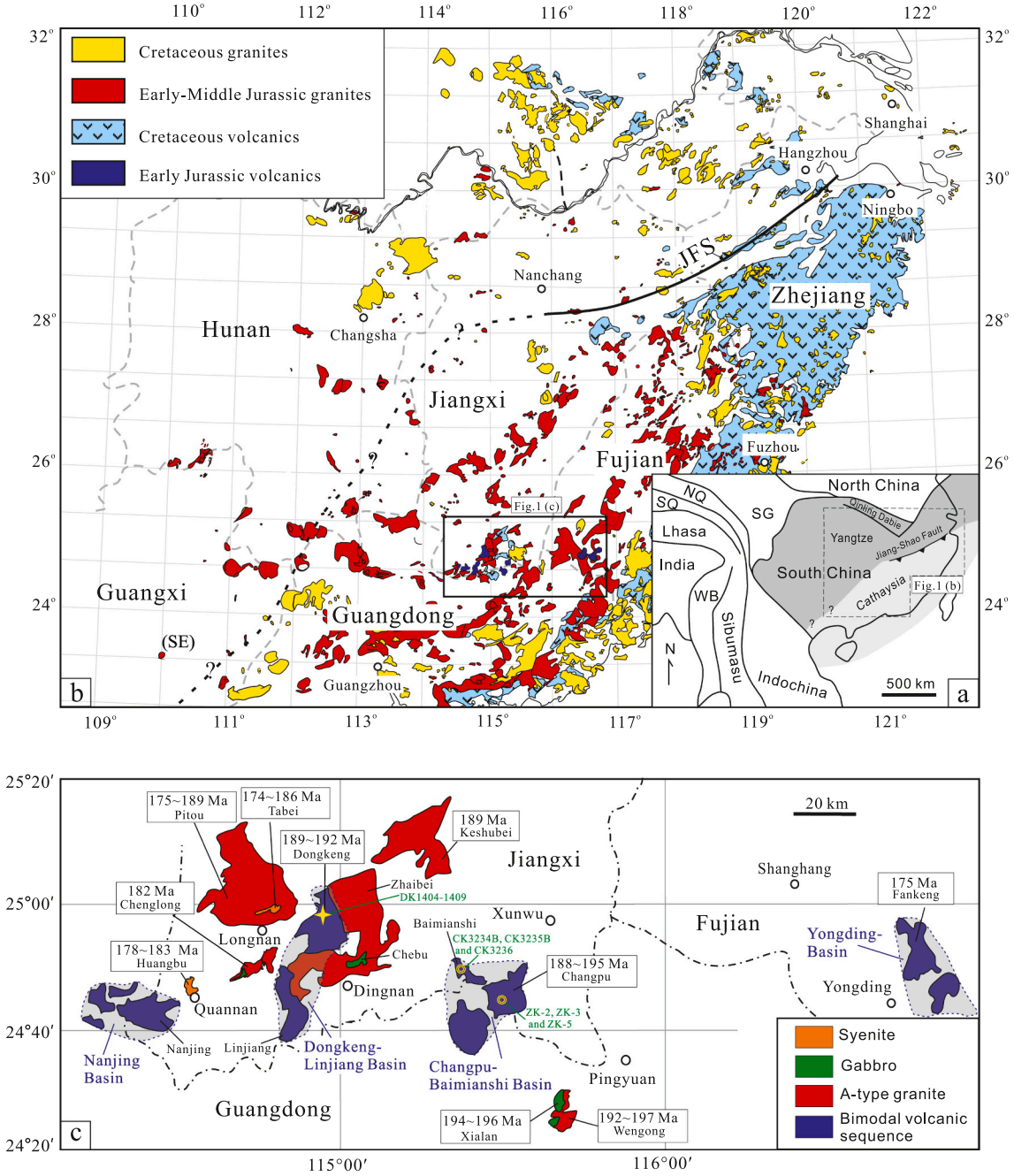

Fig. 1. (a) Geological map showing the major tectonic units in southeastern China (after Metcalfe, 2013). JSF = Jiangshan–Shaoxing Fault. (b) Distribution of Jurassic–Cretaceous volcanic rocks and granites in southeastern China (modified after Zhou et al., 2006; Cen et al., 2016). (c) Distribution of Early–Middle Jurassic volcanic and intrusive rocks in the Nanling Range in southeastern China (modified after the 1:200,000 geological map; Cen et al., 2016). Grey fields show the Early Jurassic volcanic–sedimentary basins in southern Jiangxi and southwestern Fujian provinces. Yellow double circle symbols mark the locations of the drill cores. Yellow asterisks mark the sampling sites. Data sources: Pitou granites from Chen et al. (2005) and He et al. (2010); Keshubei granites from Li and Li (2007); Tabei syenites from Chen et al. (2005) and He et al. (2010); Huangbu syenites from He et al. (2010); Chenglong gabbros from He et al. (2010); Xialan gabbros and Wengong granites from Yu et al. (2010), Zhu et al. (2010), and Gan et al. (2017a, 2017b); Dongkeng and Changpu bimodal volcanic rocks from Ji and Wu (2010), Cen et al. (2016), and Zhu et al. (2020); Yongding bimodal volcanic rocks from Zhou et al. (2005). (For interpretation of the references to colour in this figure legend, the reader is referred to the web version of this article.)

this region.

Despite numerous geochemical studies, the origin of the Early Jurassic basalts is not well understood. It is generally thought that the Early Jurassic bimodal volcanic rocks and coeval A-type granitoids and subordinate syenites in this region were generated in a continental rift or extensional setting (Bai et al., 2015; Cen et al., 2016; Chen et al., 2005; He et al., 2010; Li et al., 2003, 2004, 2007a, 2007b, 2009; Meng et al., 2012; Wang et al., 2003, 2005, 2008; Xie et al., 2006; Yu et al., 2010; Zhu et al., 2010, 2020). The Early Jurassic basalts in southern Jiangxi Province are all characterised by light rare earth element (REE) enrichments and variable negative Nb—Ta anomalies (Cen et al., 2016; Wang et al., 2005). The Sr—Nd isotope ratios of the basalts are highly variable ($\varepsilon_{Nd}(t) = +0.3$ to -4.8 and $(^{87}Sr/^{86}Sr)_i = 0.7047–0.7102$;Cen et al., 2016 ; Wang et al., 2005) and significantly enriched relative to those of the ca. 194 Ma Xialan gabbros ($\varepsilon_{Nd}(t) = +1.7$ to $+6.2$ and $^{87}Sr/^{86}Sr = 0.704–0.706$; Zhu et al., 2010), which has been explained by the earliest Jurassic mafic magmatism being generated by upwelling asthenospheric mantle (Bai et al., 2015; Gan et al., 2017a; Yu et al., 2010; Zhu et al., 2010). Thus, the key issue is whether the basalts were derived from enriched lithospheric mantle or depleted asthenospheric mantle (Wang et al., 2005; Cen et al., 2016).

Here we report for the first time whole-rock geochemical and Sr—Nd isotopic data for basalts collected from new drill cores in the Baimianshi, Changpu, and Dongkeng basins in southern Jiangxi Province. These new data and stratigraphic changes, combined with previously published geochemical data, provide new insights into the petrogenesis of the basalts and tectonic setting of Jurassic magmatism in southeast China.

2. Geological background

The South China Block (SCB) is separated from the North China Craton by the Qinling–Dabie orogenic belt to the north and is bounded by the Tibetan Plateau and Indochina Block in the west and southwest (Fig. 1a). The SCB comprises the Yangtze Block in the northwest and Cathaysia Block in the southeast, which are separated by the Jiangshan–Shaoxing fault (Fig. 1a–b; Meng et al., 2012; Cen et al., 2016). The late Mesoproterozoic to earliest Neoproterozoic Shuangxiwu arc, believed to be of Yangtze affinity, to its northwest was separated by the Jiangshan–Shaoxing fault from Cathaysian basement rocks (Li et al., 2010). The basement rocks of the Cathaysia Block comprise mid-Palaeoproterozoic (2.0–1.8 Ga) to Neoproterozoic volcanic–sedimentary rocks (Chen and Xing, 2016; Li et al., 2000; Li and Li, 2007; Yu et al., 2009), which are overlain by lower Palaeozoic metasedimentary rocks to Upper Triassic sedimentary rocks (Wan et al., 2010; Wu et al., 2000).

Late Mesozoic igneous rocks are widespread in southeastern China, including voluminous granites and volcanic rocks, and subordinate gabbros and syenites (Fig. 1b; e.g., Cen et al., 2016; He et al., 2010; He and Xu, 2012; Wang et al., 2005; Zhou et al., 2006; Zhou and Li, 2000). These rocks were generated in the Jurassic (190–155 Ma; referred to as "Early Yanshanian-aged" in the Chinese literature) and Cretaceous (145–80 Ma; referred to as "Late Yanshanian-aged" in the Chinese literature) (Fig. 1b; e.g., Li, 2000; Li et al., 2007a, 2007b, 2017; Zhou et al., 2006; Zhou and Li, 2000). The Jurassic igneous rocks are mainly distributed in the continental interior (i.e., the Nanling Range and adjacent areas), and comprise predominantly ca. 165–155 Ma large granitic plutons, and subordinate Early Jurassic (195–175 Ma) bimodal volcanic rocks, mafic intrusive rocks, and syenites (Fig. 1b–c; Li et al., 2003, 2007a, 2007b; Chen et al., 2005, 2008; Wang et al., 2005; He et al., 2010; Yu et al., 2010; Zhu et al., 2010, 2020; Meng et al., 2012; Cen et al., 2016; Gan et al., 2017a, 2017b). The Cretaceous igneous rocks occur mostly in the southeastern coastal region, and consist predominantly of silicic volcanic and intrusive rocks, along with minor amounts of mafic rocks (Fig. 1b; Zhou and Li, 2000; Zhou et al., 2006; He and Xu, 2012; Li et al., 2017).

The Early Jurassic bimodal volcanic/intrusive rocks are best exposed in the region from southern Hunan, through southern Jiangxi and northern Guangdong, to southwestern Fujian provinces (Fig. 1b–c). They consist mainly of volcanic rocks (basalts and rhyolites) and A-type granites, with subordinate syenites and gabbros (Cen et al., 2016; Chen et al., 2005; He et al., 2010; Li et al., 2003; Meng et al., 2012; Wang et al., 2003, 2005, 2008; Yu et al., 2010; Zhou et al., 2005; Zhou and Li, 2000; Zhu et al., 2020). Well-preserved bimodal volcanic rocks are exposed in the Changpu–Baimianshi, Dongkeng–Linjiang, and Nanjing volcanic–sedimentary basins in southern Jiangxi Province, and the Yongding Basin in southwestern Fujian Province (Fig. 1c).

The Early Jurassic volcanic–sedimentary sequence in the Baimianshi, Changpu, and Dongkeng basins is termed as the Yutian Group, which unconformably overlies Precambrian metamorphic rocks, Palaeozoic sedimentary rocks, and Triassic granites (Wu et al., 2000). The Yutian Group is >800–1000 m in thickness and consists predominantly of subalkaline basaltic rocks (basalts and basaltic andesites), rhyolites, sandstones, and minor high-Mg andesites–dacites (Fig. 2a; Wu et al., 2000; Zhang et al., 2002; Wang et al., 2005;Cen et al., 2016 ; Zhu et al., 2020). Rhyolites from the Changpu Basin and dacites from the Dongkeng Basin have been dated at 195 and 191 Ma, respectively (Ji and Wu, 2010). Recent zircon U—Pb dating has revealed that the rhyolites in the Changpu and Dongkeng basins formed at 190–188 Ma (Cen et al., 2016; Zhu et al., 2020). It appears that the volcanic rocks in the Changpu and Dongkeng basins were erupted in a short period in the earliest Jurassic.

The main volcanic–sedimentary sequence of the Yutian Group in the Baimianshi, Changpu, and Dongkeng basins can be divided into four volcanic units (Unit I to IV) from base to top (Fig. 2a), implying that these earliest Jurassic basalts were formed by at least four magmatic stages. The Baimianshi Basin contains mainly Unit I, II, and the lower–middle part of Unit III (Fig. 2a–b). The Changpu Basin contains mainly Unit III and IV (Figs. 2a and 3a–b). The Dongkeng Basin contains mainly the upper part of the Unit IV basalts and rhyolites (Fig. 2a). Unit I consists mainly of sandstones and basalts. Unit II includes sandstones and basalts. Unit III consists mainly of sandstones, basalts, rhyolites, and interbedded high-Mg andesites–dacites in its lower part. Unit IV consists mainly of basalts and rhyolites (Fig. 2a).

3. Sampling and petrography

Forty-one basalts were collected from the Baimianshi Basin (three drill cores: CK3234B, CK3235B, and CK3236; Figs. 1c and 2a–b), Changpu Basin (three drill cores: ZK-2, ZK-5, and ZK-3; Figs. 1c, 2a, and 3), and Dongkeng Basin (one outcrop; Figs. 1c and 2a) in southern Jiangxi Province. All the basalts are grey–black in colour, with massive or amygdaloidal structures.

Unit I basalts from the Baimianshi Basin are porphyritic and contain euhedral to sub-euhedral phenocrysts, including plagioclase (5–10 vol %) and lesser clinopyroxene. The groundmass comprises fine-grained plagioclase, clinopyroxene, and minor Fe—Ti oxides (Fig. 4a). Unit II basalts and basaltic andesites from the Baimianshi Basin consist of fine-grained plagioclase, clinopyroxene, and Fe—Ti oxides with an intergranular texture (Fig. 4b).

Most of the Unit III basalts and basaltic andesites from the Changpu Basin consist of plagioclase, clinopyroxene, and Fe—Ti oxides, with an ophitic texture (Fig. 4c). Some basalts from the Changpu Basin are porphyritic, with euhedral phenocrysts of clinopyroxene (5–15 vol%) set in a groundmass of clinopyroxene, plagioclase, and Fe—Ti oxides (Fig. 4d).

Most of the Unit IV basalts from the Changpu and Dongkeng basins have ophitic textures and consist of fine-grained plagioclase, clinopyroxene, and minor Fe—Ti oxides (Fig. 4e). Some basalts from the Changpu Basin are porphyritic and contain euhedral clinopyroxene phenocrysts (10–15 vol%). Their matrix consists mainly of clinopyroxene, plagioclase, and minor Fe—Ti oxides (Fig. 4f).

All the basaltic rocks in the Yutian Group in the Baimianshi, Changpu, and Dongkeng basins have experienced alteration to variable

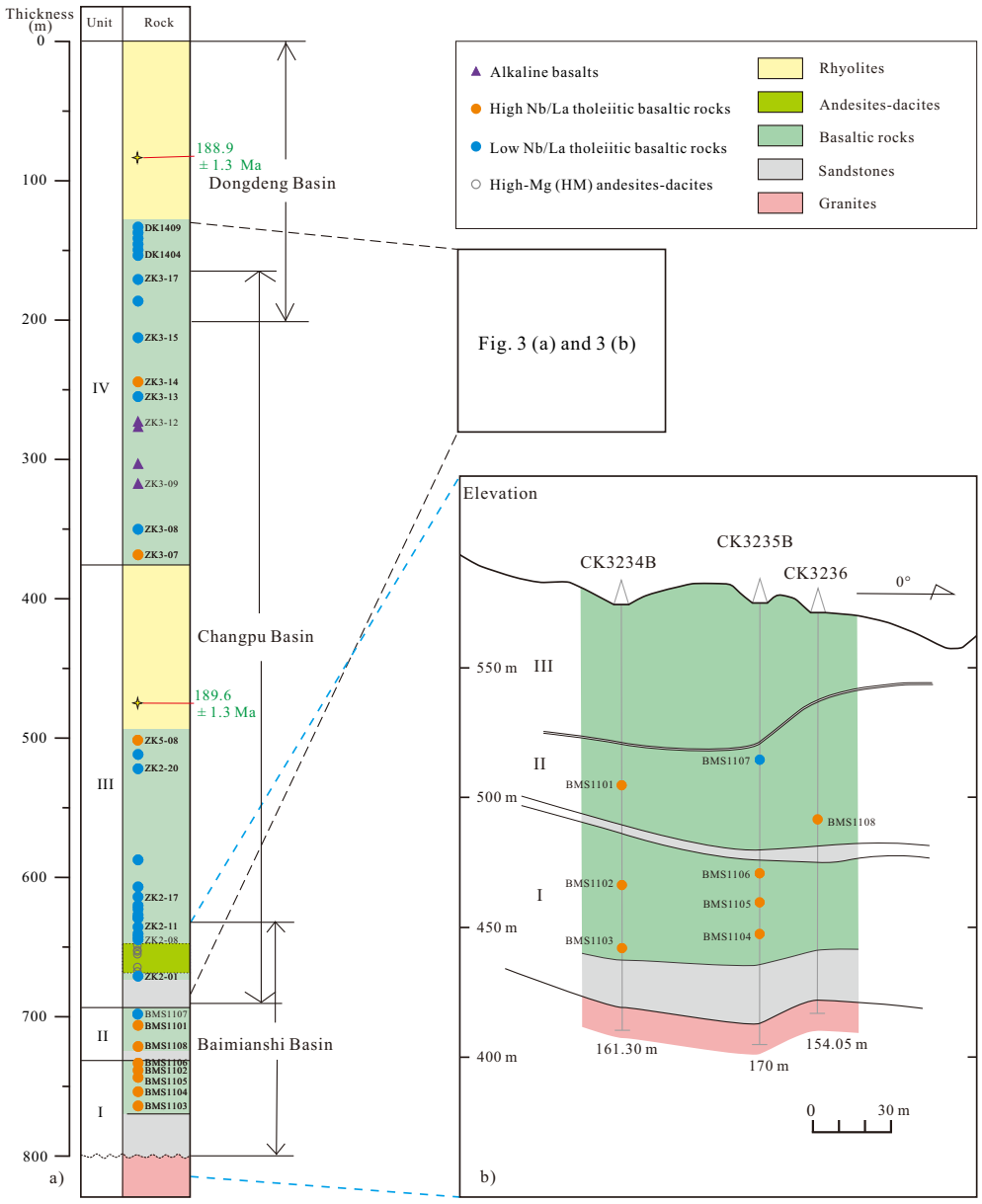

Fig. 2. (a) Simplified stratigraphy and sampling locations of the basaltic rocks in the Yutian Group in the Baimianshi, Changpu, and Dongkeng basins in southern Jiangxi Province. (b) Cross-section through boreholes CK3234B, CK3235B, and CK3236 in the Baimianshi Basin, which contain Unit I, II, and III basalts and sandstones.

degrees. The clinopyroxene phenocrysts are commonly partial chloritization, and some plagioclases have undergone carbonation alteration. In addition, the groundmass has commonly undergone indistinguishable alteration.

4. Analytical methods

Whole-rock major element compositions were determined by X-ray fluorescence spectrometry at ALS Chemex Company Ltd. in Guangzhou, China. Loss-on-ignition (LOI) values were determined on dried, powdered samples by heating to 1000 °C for 1 h and recording the weight loss. The analysed standards were the certified reference materials NIM–GBW07105, GBW07163, GBM908–10, and MRGeo08. The analytical precision is generally between ±1% and ± 5%.

Whole-rock trace element concentrations were determined with a Perkin–Elmer Sciex ELAN DRC–e inductively coupled plasma mass spectrometer (ICP-MS) at the State Key Laboratory of Ore Deposit Geochemistry, Institute of Geochemistry, Chinese Academy of Sciences (IGCAS), Guiyang, China. Dried powdered samples (50 mg) were dissolved in HF + HNO_3 in high-pressure Teflon bombs at ~190 °C for 48 h (Qi et al., 2000). Rhodium was used to monitor signal drift during the ICP-MS analyses. The analysed standards were the international reference materials BHVO-2 and BCR-2. The analytical precision is generally better than ±10%.

Dried powered samples were spiked and dissolved in Teflon bombs in HF–HNO_3–$HClO_4$ for Sr—Nd isotopic analysis. Strontium–Nd separation was undertaken by conventional cation exchange methods. The Sr—Nd concentrations and isotope ratios were determined with a Micromass Isoprobe multi-collector ICP-MS at the State Key Laboratory of Environmental Geochemistry, Institute of Geochemistry (SKLEG), Guiyang, China. The reported $^{87}Sr/^{86}Sr$ ratios were corrected for mass fractionation based on $^{86}Sr/^{88}Sr = 0.1194$. The reported $^{143}Nd/^{144}Nd$ ratios were corrected for mass fractionation based on $^{146}Nd/^{144}Nd = 0.7219$. The $^{87}Sr/^{86}Sr$ ratio determined for the SRM987 Sr standard was

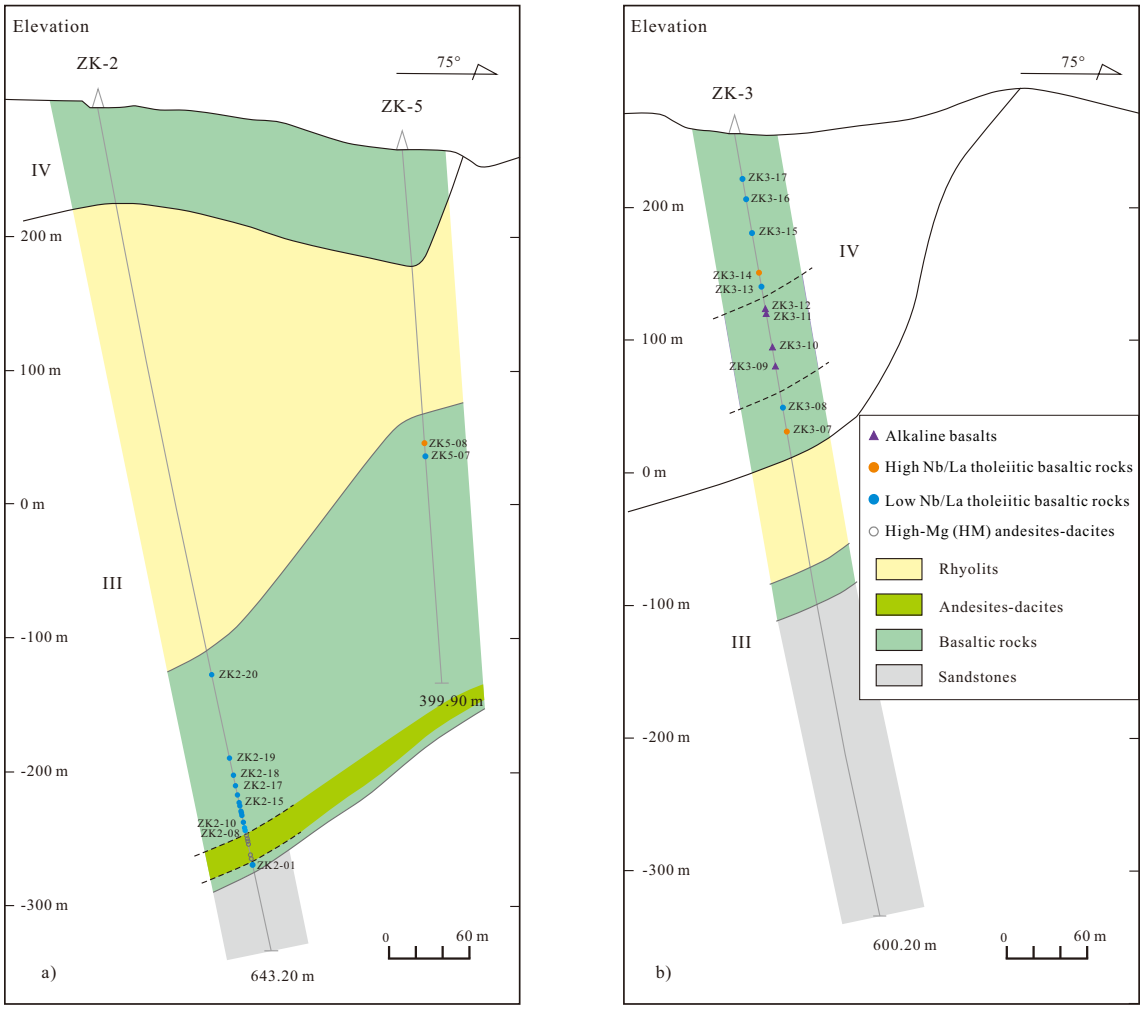

Fig. 3. Cross-section and sampling locations of basaltic rocks in (a) boreholes ZK-2 and ZK-5 and (b) borehole ZK-3 in the Changpu Basin, which contain Unit III and IV basalts, rhyolites, high-Mg andesites–dacites, and sandstones.

0.710250 ± 7 (2σ). $^{143}Nd/^{144}Nd$ ratios determined for the USGS standard BCR-2 and JNDI-1 Nd standard were 0.512629 ± 16 (2σ) and 0.512119 ± 14 (2σ), respectively. These standard values are consistent with their recommended values.

5. Results

Major and trace element data for the basaltic rocks from the Baimianshi, Changpu, and Dongkeng basins are presented in Table S1. Samples have experienced variable degrees of alteration, which is evident from the LOI values of 1.13–11.0 wt%. The effects of alteration on TiO_2 contents and trace element variation have firstly been evaluated. Zirconium in mafic igneous rocks is commonly considered to be immobile during low- to medium-grade metamorphism (e.g., Gibson et al., 1982; Wood et al., 1979). A number of elements with different geochemical behavior, including Rb, Sr, V, TiO_2, Ba, Ce, Th, Nb, and Y, were plotted versus Zr to evaluate their mobility during alteration (Fig. S1). Apart from Rb, Sr and V, the other elements are tightly correlated with Zr, suggesting that these elements were essentially immobile during alteration. Moreover, the major elements (except for TiO_2) of fourteen basaltic rocks with LOI >4.9% were not be used to discuss their petrogenesis. The major elements of the other samples with LOI <4.9% were recalculated to volatile-free basis. SiO_2, MgO, Fe_2O_3, Al_2O_3, CaO, and P_2O_5 contents (volatile-free) of the samples with LOI <4.9% exhibit fairly constant with increasing LOI contents (Fig. S2), suggesting that the major elements were rather immobile during alteration. In addition, SiO_2 contents (volatile-free) increase, whereas MgO and CaO contents of these rocks decrease with increasing TiO_2 and Zr contens (Figs. S3 and S4), implying that these elements variation were affected by some degrees of fractionation of mafic minerals rather than the alteration. Therefore, these immobile major and trace elements can be used for geochemical classification and petrogenetic interpretations.

5.1. Rock types and stratigraphy

Based on Zr/TiO_2 and Nb/Y ratios (Fig. 5a; Winchester and Floyd, 1976), the basaltic rocks from the Baimianshi, Changpu, and Dongkeng basins can be divided into two compositional groups, including subalkaline (Nb/Y < 0.80) and alkaline basalts (Nb/Y > 0.80). In plots of TiO_2 versus FeO*/MgO (Fig. 5b; Miyashiro, 1974) and FeO*/MgO versus SiO_2 (Fig. 5c; Miyashiro, 1974), all the subalkaline basalts have tholeiitic affinities. The alkaline basalts have relatively higher Ti/Y and La/Yb ratios, and lower Th/Nb ratios than those of the tholeiitic basaltic rocks (Fig. 6a–c). Thus, these basaltic rocks, showing distinctive geochemical features, can be divided into two rock types: alkaline basalts and tholeiitic basalts (Figs.5 and 6 a–c).

The studied samples are mostly tholeiitic basaltic rocks, with subordinate alkaline basalts (Fig. 5; Table S1). It is noted that the published basaltic rocks from Wang et al. (2005) and Cen et al. (2016) are mainly the tholeiitic basaltic rocks (Fig. 6). The Unit I, Unit II and Unit III basalts are all the tholeiitic basaltic rocks. Unit IV basalts comprise mainly the tholeiitic basaltic rocks interbedded with subordinate alkaline basalts in

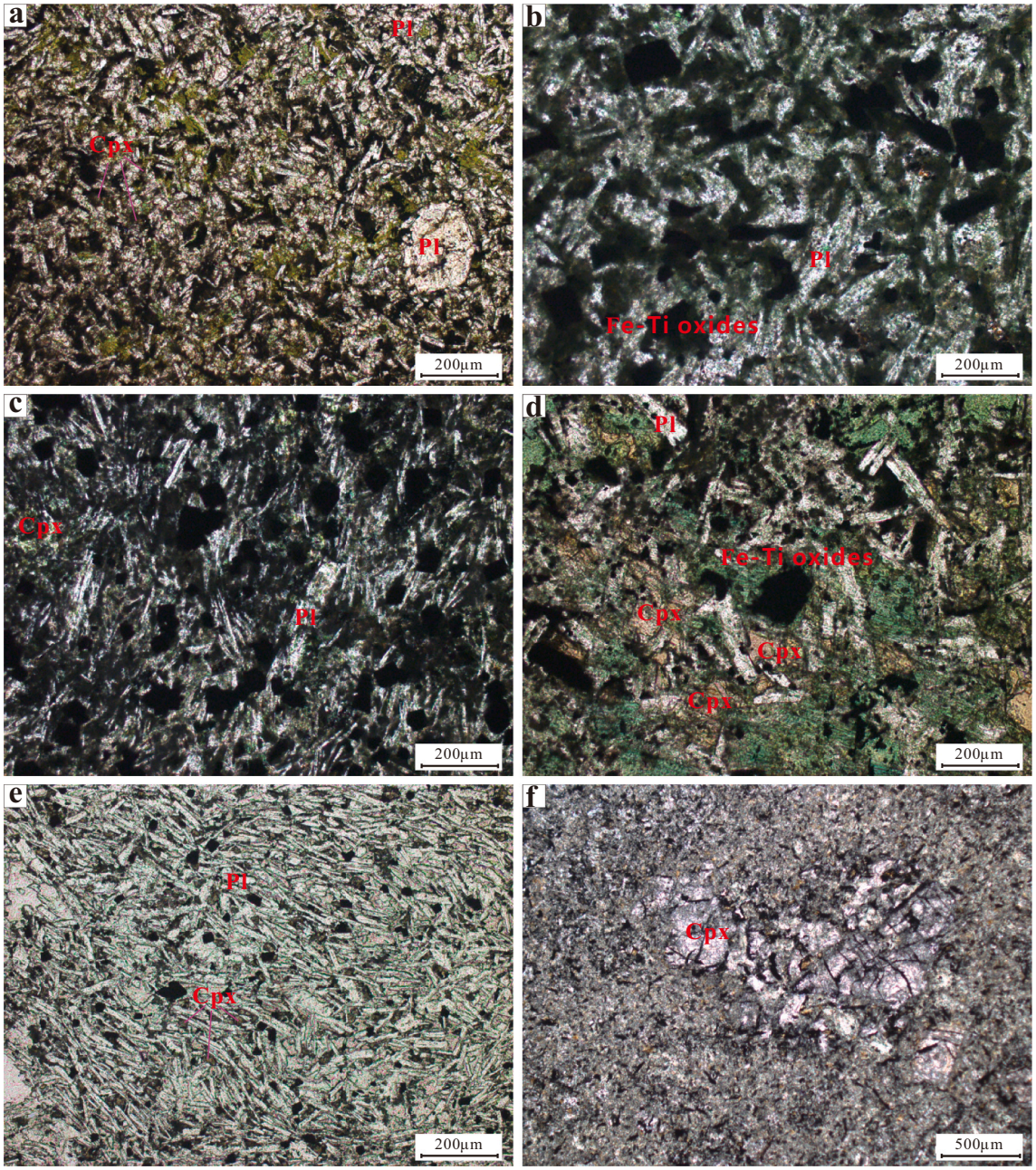

Fig. 4. Photographs of representative basaltic rocks from the Baimianshi, Changpu, and Dongkeng basins. (a) BMS1102 (Unit I basalt); (b) BMS1107 (Unit II basaltic andesite); (c) ZK2–10 (Unit III basalt); (d) ZK5–08 (Unit III basalt); (e) ZK3–09 (Unit IV basalt); (f) ZK3–14 (Unit IV basalt). Mineral abbreviations: Pl = plagioclase; Cpx = clinopyroxene.

its lower–middle part (Figs. 2–3).

5.2. Major and trace elements

The alkaline basalts have a narrow range of major element and high TiO_2 and P_2O_5 contents (TiO_2 = 3.13–4.19 wt%; P_2O_5 = 0.69–1.15 wt %), with Mg# = 45–48, MgO = 6.71–6.83 wt%, SiO_2 = 44.7–47.6 wt%, $Fe_2O_3^T$ = 14.5–16.5 wt%, Al_2O_3 = 15.1–15.7 wt%, CaO = 6.50–9.74 wt %, Cr = 19.9–112 ppm, and Ni = 27.3–73.6 ppm (Table S1; Figs. 7 and 8a). Moreover, the alkaline basalts have high Ti/Y (596–699; Figs. 6a and 8b) and Nb/Y ratios (0.85–0.92; Figs. 5a and 8c).

Unlike the alkaline basalts, the tholeiitic basalts have a relatively wide range of major and compatible trace element contents (e.g., Cr and Ni). The tholeiitic basalts have Mg# = 28–57, MgO = 2.92–8.37 wt%, SiO_2 = 47.5–57.2 wt%, TiO_2 = 1.26–3.26 wt%, $Fe_2O_3^T$ = 11.4–15.6 wt %, Al_2O_3 = 13.7–18.1 wt%, CaO = 3.00–10.1 wt%, P_2O_5 = 0.24–0.52 wt %, Cr = 3.97–764 ppm, and Ni = 2.08–228 ppm (Table S1; Figs. 7 and 8a). CaO, Cr, and Ni contents of the tholeiitic basalts decrease with decreasing MgO, whereas SiO_2, TiO_2, and P_2O_5 contents increase (Fig. 7). In addition, the tholeiitic basalts have relatively low Ti/Y (135–534; Figs. 6a and 8b) and Nb/Y ratios (0.32–0.69; Figs. 5a and 8c).

In chondrite-normalised REE plots (Fig. 9a), the alkaline basalts have relatively high total REE contents (La = 26.0–38.2 ppm; ΣREE = 148–212 ppm) and light REE (LREE)-enriched and heavy REE (HREE)-depleted patterns (La/Yb = 13.5–14.3, La/Sm = 4.1–4.3, and Sm/Yb = 3.2–3.3), and no significant Eu anomalies (Eu/Eu* = 1.0–1.1). In primitive-mantle-normalised diagrams (Fig. 9b; Boynton, 1984), the alkaline basalts have patterns characterised by variable enrichments in

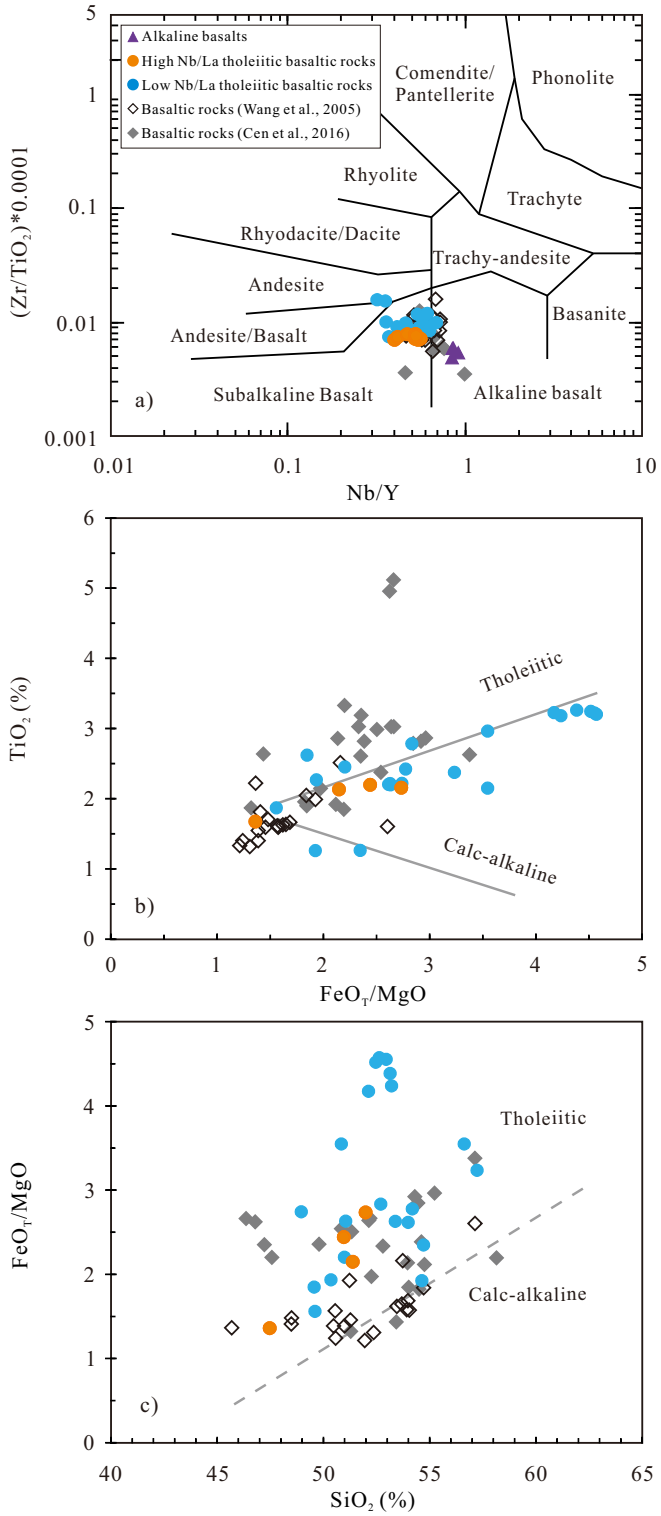

Fig. 5. Plots of (a) Zr/TiO_2 vs. Nb/Y (Winchester and Floyd, 1976), (b) TiO_2 vs. FeO_T/MgO (Miyashiro, 1974), and (c) FeO_T/MgO versus SiO_2 (Miyashiro, 1974) for classification of the basaltic rocks from the Baimianshi, Changpu, and Dongkeng basins. Published data for the basalts are from Wang et al. (2005) and Cen et al. (2016).

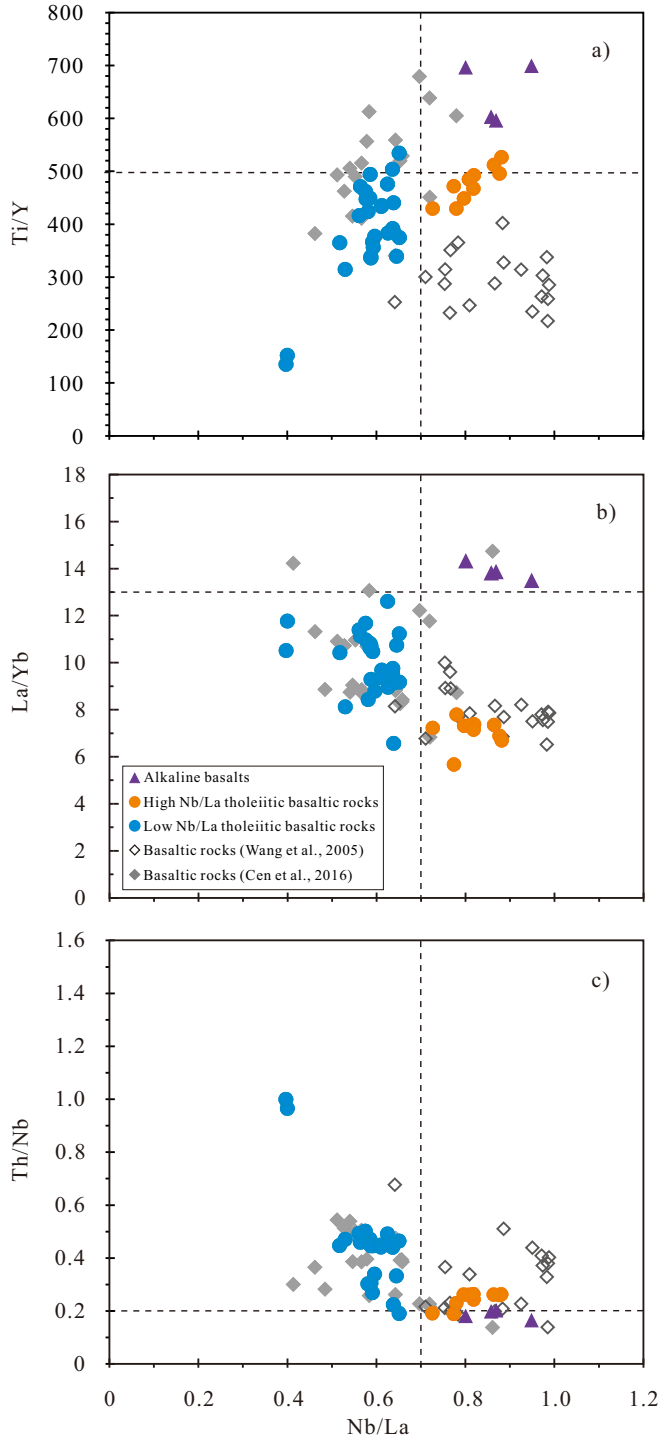

Fig. 6. Plots of (a) Ti/Y, (b) La/Yb, and (c) Th/Nb vs. Nb/La for the basaltic rocks from the Baimianshi, Changpu, and Dongkeng basins. Published data for the basaltic rocks are from Wang et al. (2005) and Cen et al. (2016).

all incompatible elements. The alkaline basalts have negligible to slightly negative Nb—Ta anomalies relative to La (Nb/La = 0.80–0.95; Figs. 6, 8d, and 9b) and resemble typical intraplate alkaline basalts from continental flood basalt (CFB) and ocean island basalt (OIB) provinces (Sun and McDonough, 1989).

Compared with the alkaline basalts, the tholeiitic basalts have variable total REE contents and are moderately to strongly LREE-enriched and HREE-depleted, with insignificant to slightly negative Eu anomalies (Fig. 9c). In terms of primitive-mantle-normalised trace element patterns (Fig. 9d), the tholeiitic basalts exhibit variable enrichments in all incompatible elements with small–large Nb–Ta–Ti–P depletions relative to neighbouring elements (Nb/La = 0.40–0.88; Figs. 6, 8d, and 9d). Based on their Nb/La ratios, the tholeiitic basaltic rocks can be further

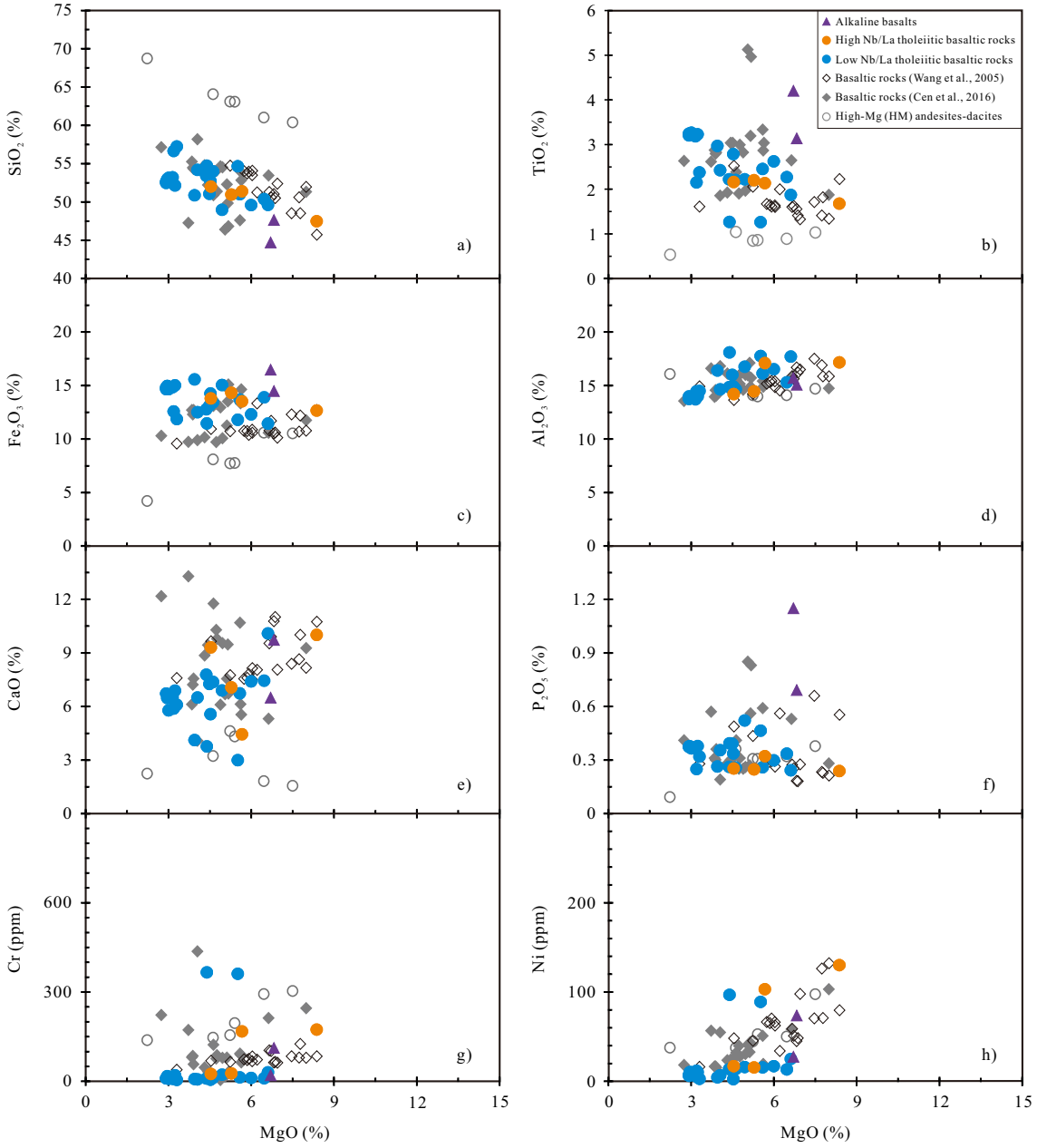

Fig. 7. Plots of (a) SiO_2, (b) TiO_2, (c) Fe_2O_3, (d) Al_2O_3, (e) CaO, (f) P_2O_5, (g) Cr, and (h) Ni vs. MgO for basaltic rocks with LOI < 4.9% from the Baimianshi, Changpu, and Dongkeng basins. Published data for the basaltic rocks are from Wang et al. (2005) and Cen et al. (2016). Published data for the high-Mg andesites–dacites are from Zhu et al. (2020).

divided into two sub-types: a high Nb/La group (Nb/La > 0.70) and a low Nb/La group (Nb/La < 0.70) (Fig. 6a–c). The high Nb/La tholeiitic basaltic rocks also show relatively lower La/Yb and Th/Nb ratios than those of the low Nb/La tholeiitic basaltic rocks (Fig. 6b–c).

The high Nb/La tholeiitic basaltic rocks show relatively low total REE contents (La = 11.0–20.0 ppm, REE = 71.2–126 ppm) with moderately LREE-enriched and relatively flat HREE-depleted patterns (La/Yb = 5.7–7.8, La/Sm = 2.7–3.4, Sm/Yb = 2.1–2.3) and negligibly to slightly negative Eu anomalies (Eu/Eu* = 0.8–1.1) (Figs. 8e and 9c). In the primitive mantle-normalised spider diagram (Fig. 9d; Sun and McDonough, 1989), the high Nb/La tholeiitic basaltic rocks exhibit slight–moderate enrichments in all the incompatible elements with insignificantly-weakly Nb–Ta–Ti anomalies depletion relative to their neighbouring elements (Nb/La = 0.73–0.88; Figs. 6, 8d, and 9d). The trace element patterns of the high Nb/La tholeiitic basaltic rocks vary between E-MORB and OIB (Fig. 9d).

Compared with the high Nb/La tholeiitic basaltic rocks, the low Nb/La tholeiitic basaltic rocks have high and variable total REE contents (La = 11.1–45.1 ppm, REE = 69.5–235 ppm) with moderately–strongly LREE-enriched and HREE-depleted patterns (La/Yb = 6.6–12.6, La/Sm = 3.5–5.1, Sm/Yb = 1.9–2.9), and insignificantly to slightly negative Eu anomalies (Eu/Eu* = 0.7–1.1) (Figs. 8e and 9c). In terms of primitive mantle-normalised trace element patterns (Fig. 9d; Sun and McDonough, 1989), the low Nb/La tholeiitic basaltic rocks show "humped" patterns characterised by variable enrichment in all incompatible elements with moderately to strongly negative Nb—Ta anomalies relative to La (Nb/La = 0.40–0.65) and variable Ti depletion relative to adjacent trace elements (Figs. 6, 8d, and 9d). It is noticed that the low Nb/La tholeiitic basaltic rocks with moderate Nb—Ta depletion are similar to those of the high Nb/La tholeiitic basaltic rocks, whereas the low Nb/La

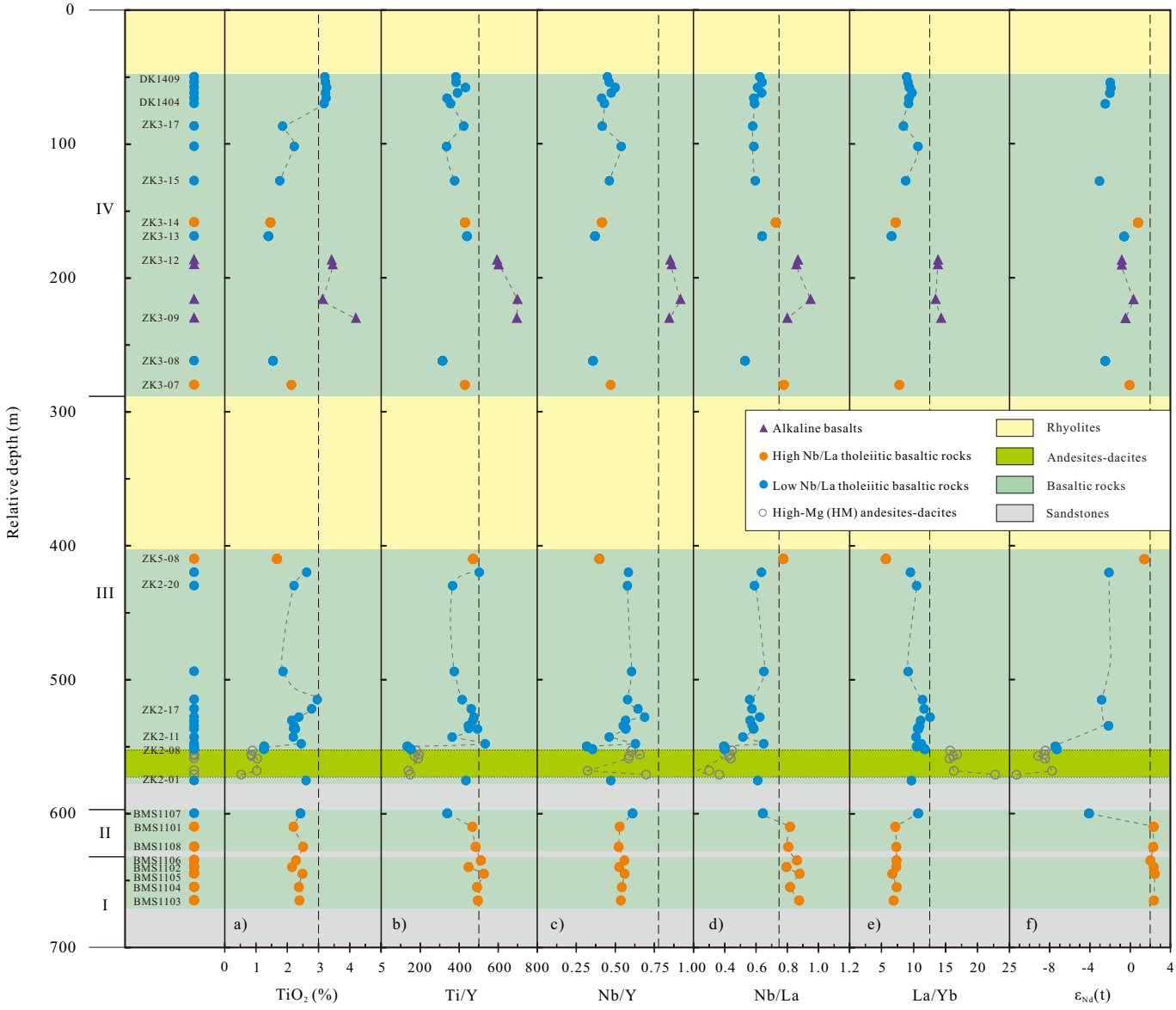

Fig. 8. Stratigraphic variations of (a) TiO_2 contents, (b) Ti/Y ratios, (c) Nb/Y ratios, (d) Nb/La ratios, (e) La/Yb ratios, and (f) $\varepsilon_{Nd}(t)$ values for the basaltic rocks from the Baimianshi, Changpu, and Dongkeng basins. Published data for the high-Mg andesites–dacites are from Zhu et al. (2020).

tholeiitic basaltic rocks with large negative Nb—Ta anomalies (Nb/La < 0.5) and variable Ti depletions relative to adjacent trace elements, remarkably resemble those of island arc basalts (IABs) and are very similar to those of the Changpu high-Mg andesites–dacites (Fig. 9d). Thus, the trace element contents of the low Nb/La tholeiitic basalts vary mostly between E-MORB and the Changpu high-Mg andesites–dacites' compositions (Fig. 9d).

5.3. Sr—Nd isotopes

Whole-rock Sr—Nd isotopic compositions of 26 basaltic rocks from the Baimianshi, Changpu, and Dongkeng basins are presented in Table S2. The alkaline basalts have primitive mantle-like $\varepsilon_{Nd}(t)$ values of −0.85 to +0.33 and moderately elevated $(^{87}Sr/^{86}Sr)_i$ ratios of 0.7074–0.7082. The high Nb/La tholeiitic basaltic rocks exhibit mostly positive high $\varepsilon_{Nd}(t)$ values from −0.04 to +2.5 and slightly elevated $(^{87}Sr/^{86}Sr)_i$ ratios of 0.7061–0.7088. In contrast, the low Nb/La basaltic rocks are characterised by significantly lower $\varepsilon_{Nd}(t)$ values of −7.4 to −0.60 and higher initial $(^{87}Sr/^{86}Sr)_i$ ratios of 0.7082–0.7115 than those of the high Nb/La tholeiitic basaltic rocks (Table S2; Figs. 8f and 10).

6. Discussion

6.1. Crystal fractionation

The alkaline basalts are characterised by rather constant major and trace elements contents (Figs. 7 and 9a–b), suggesting that they have undergone minor amounts of fractional crystallisation.

In contrast, the high Nb/La and low Nb/La tholeiitic basaltic rocks have variable MgO, SiO_2, Cr, and Ni contents, and exhibit coherent trends on Fenner diagrams (Fig. 7), indicating that the parental magmas of these rocks had experienced similar fractional crystallisation to varying degrees. Increase of TiO_2 and Fe_2O_3 with decreasing MgO contents for these rocks indicates that Fe—Ti oxides were not a fractionated phase (Fig. 7b–c). The positive correlations of Cr and Ni versus MgO imply that they were subjected to some degrees of olivine and clinopyroxene fractionation (Fig. 7g–h). Furthermore, the tholeiitic basalts display an obvious decrease in CaO contents and CaO/Al_2O_3

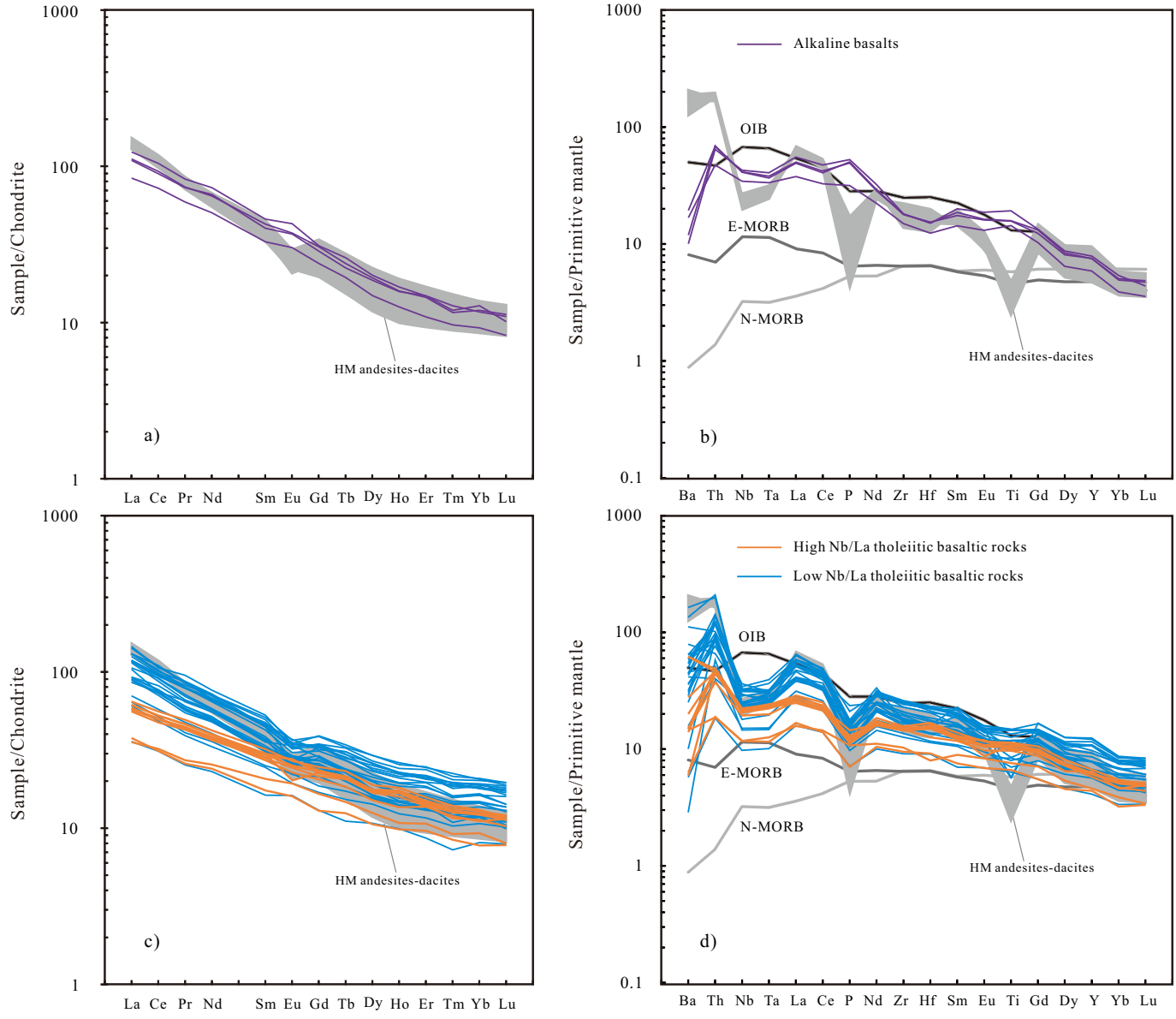

Fig. 9. Chondrite-normalised REE and primitive-mantle-normalised incompatible trace element patterns for the (a, b) alkaline basalts, and (c, d) tholeiitic basaltic rocks from the Baimianshi, Changpu, and Dongkeng basins. Data sources: chondrite-normalising values were taken from Boynton (1984); trace element data for primitive mantle (PM), ocean island basalts (OIBs), N-type mid-ocean ridge basalts (N-MORBs), and *E*-type MORBs are from Sun and McDonough (1989); trace element data for the high-Mg andesites–dacites are from Zhu et al. (2020).

ratios and slight decrease in Al_2O_3 contents with decreasing MgO, as well as slightly negative Eu anomalies (Fig. 7 d–e), which are consistent with some degrees of fractionation of clinopyroxene with insignificant plagioclase fractionation. Thus, olivine and clinopyroxene were the major fractionating minerals in the tholeiitic basalts.

6.2. Crustal contamination

The alkaline basalts have nearly constant and slight depletions of Nb—Ta relative to La and Th (Nb/La = 0.80–0.95; Figs. 6, 8d, and 9b). These basalts also have relatively uniform Sr—Nd isotopic compositions ($(^{87}Sr/^{86}Sr)_i$ = 0.7074–0.7082 and $\varepsilon_{Nd}(t)$ = −0.85 to +0.33; Table S2; Figs. 8f and 10). In addition, Nb/La, La/Yb, La/Sm, and Th/Nb ratios of these rocks show no significant changes with decreasing $\varepsilon_{Nd}(t)$ values (Figs. 11a–d), suggesting that their parental magmas did not experience significant crustal contamination.

The high Nb/La tholeiitic basaltic rocks are characterised by small Nb—Ta depletions (Nb/La = 0.73–0.88; Figs. 6, 8d, and 9d) and relatively high $\varepsilon_{Nd}(t)$ values of −0.04 to +2.5 and low initial $(^{87}Sr/^{86}Sr)_i$ (0.7061–0.7088) (Figs. 8f and 10; Table S2). Thus, the high Nb/La tholeiitic basalts may have undergone limited crustal contamination and were possibly derived from the depleted asthenospheric mantle.

In contrast, the low Nb/La tholeiitic basalts with moderate to large negative Nb–Ta–Ti anomalies (Nb/La = 0.40–0.65; Figs. 6, 8d, 9d and 11a) have relatively low $\varepsilon_{Nd}(t)$ values of −7.4 to −0.60 and high initial $(^{87}Sr/^{86}Sr)_i$ values (0.7082–0.7115) (Figs. 8f, 10 and 11; Table S2). These low Nb/La basalts also have relatively higher La/Yb, La/Sm, Th/Nb, Ba, and Ba/Nb values than those of the high Nb/La tholeiitic basalts with small Nb—Ta depletions (Fig. 11b–e). It is noted that two low Nb/La tholeiitic basaltic rocks (samples ZK2–08 and ZK2–09; termed "high-Ba tholeiitic basalts" in this study) have exceptionally high Ba and Th concentrations (Table S1; Fig. S1e and g; Ba = 949–1150 ppm, Th = 17.0–17.9 ppm). The two high-Ba basaltic rocks also have very low TiO_2 contents (1.26 wt%; Fig. 8a), Ti/Y (135–152; Fig. 8b), and Nb/Y ratios

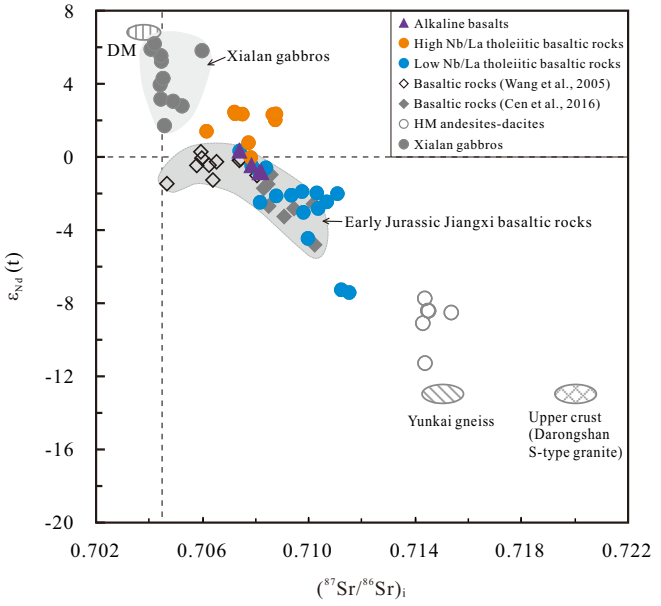

Fig. 10. Plot of initial $\varepsilon_{Nd}(t)$ vs. $(^{87}Sr/^{86}Sr)_i$ for the basaltic rocks from the Baimianshi, Changpu, and Dongkeng basins. The Sr—Nd isotopic compositions of the upper crust ($\varepsilon_{Nd}(t) = -13$, and $(^{86}Sr/^{87}Sr)_i = 0.720$) are similar to that of the S-type Darongshan granites (Jiao et al., 2015; Qi et al., 2007; Yu et al., 1999). The Sr—Nd isotopic compositions of the country rocks ($\varepsilon_{Nd}(t) = -13$, and $(^{87}Sr/^{86}Sr)_i = 0.715$) are that of metasedimentary rocks (i.e., gneisses) in the Yunkai Group in the Cathaysia Block (Wan et al., 2010). Data sources: Sr—Nd isotopic data for Early Jurassic Jiangxi basaltic rocks are from Wang et al. (2005) and Cen et al. (2016); Sr—Nd isotopic data for Early Jurassic Xialan gabbros are from Zhu et al. (2010); Sr—Nd isotopic data for Early Jurassic high-Mg andesites–dacites are from Zhu et al. (2020).

(0.32–0.35; Fig. 8c). Moreover, the high-Ba rocks exhibit strong depletions in Nb–Ta–Ti–P relative to neighbouring elements (Nb/La = 0.40; Figs. 6, 8d, 9b and 11a) and low $\varepsilon_{Nd}(t)$ values of −7.3 to −7.4 (Figs. 8f, 10, and 11). In general, the basalts with significantly negative Nb–Ta–Ti anomalies may have experienced large amounts of crustal contamination (Arndt and Christensen, 1992; Rudnick and Fountain, 1995) or have been generated by melting of metasomatised lithospheric mantle (e.g., Donnelly et al., 2004; Tang et al., 2012).

Based on the $\varepsilon_{Nd}(t)$ values, Nb/La, and La/Sm ratios, we conducted quantitative modelling of crustal assimilation by the low Nb/La tholeiitic basalts with moderate–large Nb—Ta depletions. The high Nb/La tholeiitic basalt (sample BMS1105) was chosen to represent the least-contaminated tholeiitic basalt that was derived from the depleted asthenospheric mantle. The compositions of lower Palaeozoic metasedimentary rocks (i.e., gneisses) from the Yunkai Group (Wan et al., 2010) were used for the country rocks (i.e., the potential crustal contaminants). The modelling results are shown in Fig. 11a and c. It appears that 10% to 50% contamination by such crustal components is needed to account for the $\varepsilon_{Nd}(t)$, Nb/La, and La/Sm variations exhibited by the low Nb/La tholeiitic basalts. Especially, the calculation suggests that up to 50% crustal contamination is needed to amount for the compositional variations observed in the high-Ba tholeiitic basalts with large Nb—Ta depletions. However, these modelling results are not consistent with the bulk compositions (e.g., SiO_2 contents) of the basalts given the large amounts of assimilation of felsic crust required to produce the Nd isotopic and trace elemental variations. Therefore, crustal contamination had an insignificant role in the formation of the low Nb/La tholeiitic basalts with moderate–large Nb—Ta depletions. In fact, the trends in Fig. 11 likely record hybridisation between the parental magmas of the high Nb/La tholeiitic basalts and the high-Ba tholeiitic basalts.

In summary, the contribution of crustal contamination in the generation of the alkaline and tholeiitic basalts was most likely limited.

6.3. Nature of the parental magmas and mantle sources

The alkaline basalts have a high-Ti alkaline basalt affinity (Figs. 6a, and 8a–b). They have OIB-like trace element features similar to alkaline basalts in continental rifts (Fig. 9a–b), such as in the modern East African Rift (Pik et al., 1999; Stewart and Rogers, 1996) and the 803 Ma Suxiong alkaline basalts in the Kangding Rift in South China (Li et al., 2002). One alkaline basalt has a slightly depleted $\varepsilon_{Nd}(t)$ value of +0.33 (Figs. 8f and 10; Table S2), suggesting that the parental magmas of the alkaline basalts were generated from a slightly depleted mantle source. Given that La and Sm are incompatible in garnet, whereas Yb is compatible, high La/Yb and Sm/Yb ratios are indicative of a small degree of melting and/or garnet as a residual phase in the source (e.g., Deniel, 1998; Green, 1994; Jenner et al., 1990). On the plot of $(Sm/Yb)_{PM}$ versus $(Th/Nb)_{PM}$ (Fig. 12a), the alkaline basalts exhibit high $(Sm/Yb)_{PM}$ and low $(Th/Nb)_{PM}$ ratios, which reflects the presence of residual garnet during partial melting of the slightly depleted mantle source. Moreover, these alkaline basalts show relatively high La/Sm, Gd/Yb, and $(Tb/Yb)_{PM}$ ratios (Fig. 12b–c), also suggesting that garnet in the partial melting residue, a feature of small-degree partial melting at a high depth. In addition, the alkaline basalts have relatively high Sm/Yb ratios and Sm contents, suggesting that they were generated by relatively low degree (& 5%–7%) of partial melting of a slightly depleted mantle source at the depth within the garnet–spinel stability field with more garnet than spinel (Fig. S5; Lassiter and DePaolo, 1997).

Unlike the alkaline basalts, the tholeiitic basaltic rocks show low-Ti tholeiitic basaltic features (Figs. 5, 6a, and 8a–b). The high Nb/La tholeiitic basalts with small negative Nb—Ta anomalies (Figs. 6, 8d, and 9d) have relatively high $\varepsilon_{Nd}(t)$ values (−0.04 to +2.5; Figs. 8f, 10 and 11; Table S2). This suggests that the parental melts of the high Nb/La tholeiitic basalts were produced by a depleted asthenospheric mantle source. These basalts show relatively lower $(Sm/Yb)_{PM}$, La/Sm, Gd/Yb, $(Tb/Yb)_{PM}$ ratios, and Sm contents than those of the alkaline basalts (Fig. 12). Moreover, the high Nb/La tholeiitic basalts show a diagonal trend between the low-degree deep melting OIB-like compositions and the high-degree shallow melting MORB-like compositions (Fig. 12b–c). We speculate that the high Nb/La tholeiitic basalts may derive from by moderate degrees (& 15%–20%) of partial melting of a depleted asthenospheric mantle source at a shallow depth, likely within the garnet–spinel stability field (Fig. S5; Lassiter and DePaolo, 1997).

In contrast, the trace element contents of low Nb/La tholeiitic basalts exhibit moderate to large negative Nb—Ta anomalies (Figs. 6, 8d, 9d and 11). The trace elemental and Nd isotopic features of the low Nb/La tholeiitic basaltic rocks with moderate Nb—Ta depletion are very similar to those of the high Nb/La tholeiitic basaltic rocks (Fig. 9c–d), implying that the magmas parental to these rocks were mainly derived from a depleted asthenospheric mantle source. However, the high-Ba tholeiitic rocks with large Nb–Ta–Ti depletions (Nb/La = 0.40; Figs. 6, 8d, and 9b) are similar to IABs (Kepezhinskas et al., 1996). Previous studies have shown that subducted oceanic sediment-derived melts have high concentrations of Th and LREEs, whereas slab-derived fluids are characterised by high contents of LILEs (e.g., Ba, Rb, Sr, and Pb; Tatsumi and Eggins, 1995; Hawkesworth et al., 1997). The high-Ba tholeiitic basalts exhibit Th–LREE enrichment (Fig. 9c–d) and have very high Ba contents (Ba = 949–1150 ppm; Table S1; Figs. 9d, 11e, and S1e). The trace element features of these basalts are similar to the high-Mg andesites–dacites (Figs. 8 and 9c–d). In particular, the high-Ba basalts have strongly negative $\varepsilon_{Nd}(t)$ values (−7.3 to −7.4), which are also similar to those of the high-Mg andesites–dacites ($\varepsilon_{Nd}(t) = -7.8$ to −11.3; Figs. 10 and 11; Zhu et al., 2020). Previous studies have suggested that the parental magmas of the high-Mg andesites–dacites originated by interactions between subducted sediment-derived melts/fluids and the overlying mantle (e.g., Zhu et al., 2020). Therefore, the parental magmas of the high-Ba tholeiitic basalts were likely sourced from lithospheric mantle that had been metasomatised by such melts and/or fluids. The elemental and Nd isotopic variations of the low Nb/La

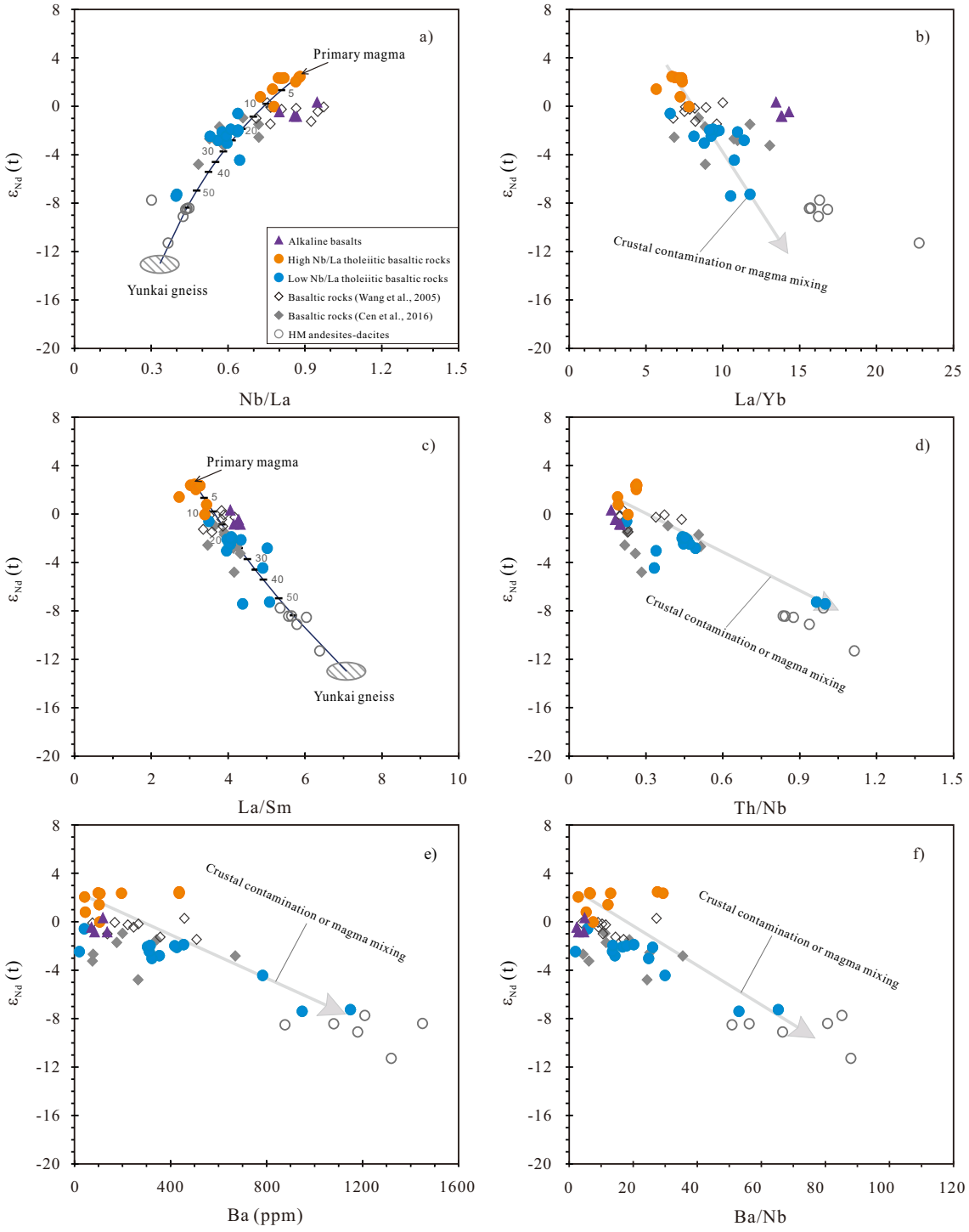

Fig. 11. Plots of $\varepsilon_{Nd}(t)$ versus (a) Nb/La, (b) La/Yb, (c) La/Sm, (d) Th/Nb, (e) Ba, and (f) Ba/Nb for basaltic rocks from the Baimianshi, Changpu, and Dongkeng basins. The primary basaltic magma of the tholeiitic basalts was assumed to have La = 18.0 ppm, Sm = 5.75 ppm, Nd = 23.0 ppm, Nb = 15.8 ppm, and $\varepsilon_{Nd}(t)$ = +2.45 (t = 189 Ma), which is similar to the least-contaminated high Nb/La basaltic sample (BMS1105). The assumed compositions of the country rocks (La = 50.3 ppm, Sm = 7.07 ppm, Nd = 35.9 ppm, Nb = 16.8 ppm, and $\varepsilon_{Nd}(t)$ = −13 (t = 189 Ma)) are similar to that of the metasedimentary rocks (i.e., gneisses) in the Yunkai Group in the Cathaysia Block (Wan et al., 2010). Published data for the basaltic rocks are from Wang et al. (2005) and Cen et al. (2016). Data for the high-Mg andesites–dacites are from Zhu et al. (2020).

tholeiitic basalts can be explained by magmas mixing between the parental magmas for the high Nb/La tholeiitic basalts and for the high-Ba tholeiitic basalts (Fig. 11).

To conclude, the parental magmas for the high-Ti alkaline basalts were produced by relatively low degrees (5%–7%) of partial melting of an asthenospheric mantle at the depth within the garnet–spinel-bearing mantle with more garnet than spinel, whereas the parental melts for the high Nb/La tholeiitic basalts were generated by moderate degrees (15%–20%) of partial melting of an asthenospheric mantle at the depth within the garnet–spinel stability field (Fig. S5). The parental magmas for the low Nb/La tholeiitic basalts with variable Nb—Ta depletions and $\varepsilon_{Nd}(t)$ values were formed by variable degrees of hybridisation between

the parental melts for the high Nb/La tholeiitic rocks and the parental melts for the high-Ba tholeiitic rocks that were derived from the overlying metasomatised lithospheric mantle (Fig. 11).

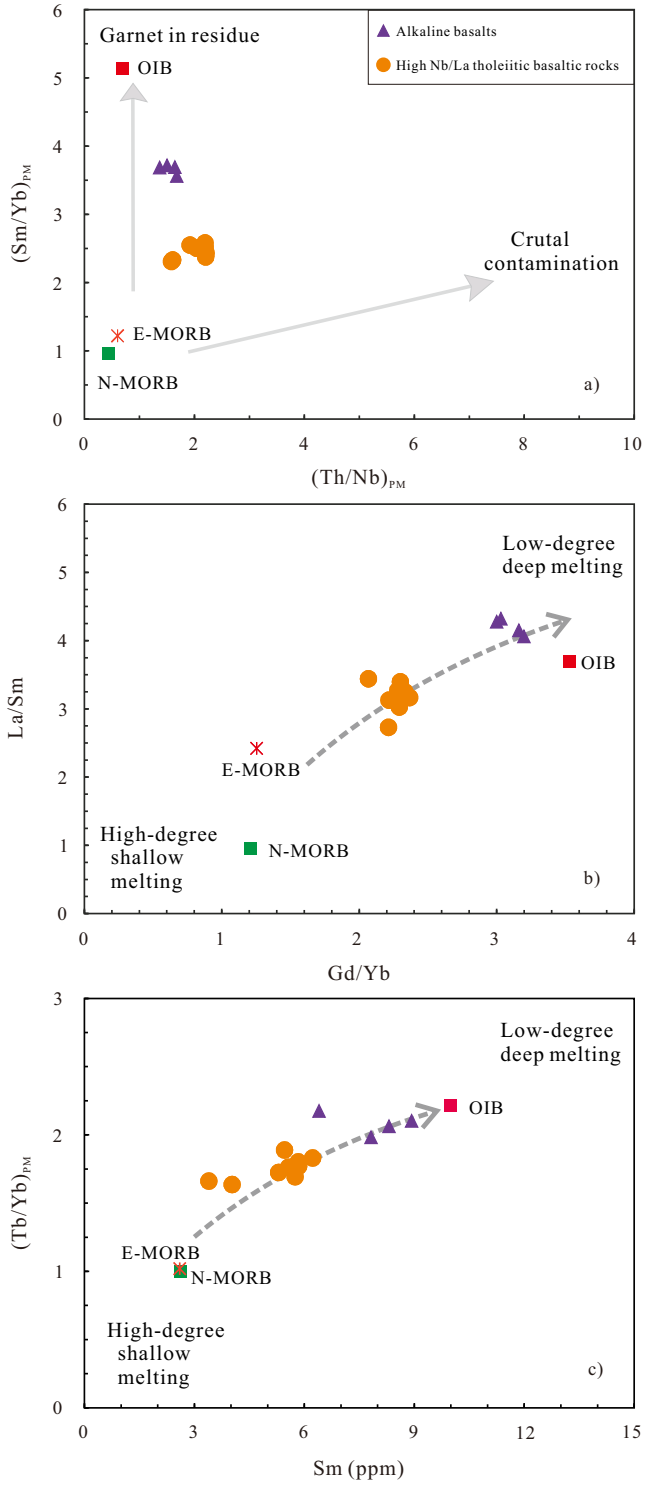

Fig. 12. Plots of $(Sm/Yb)_{PM}$ vs. $(Th/Nb)_{PM}$ ratios (a), La/Sm vs. Gd/Yb ratios (b), and $(Tb/Yb)_{PM}$ ratios vs. Sm contents (c) for the alkaline basalts and the high Nb/La tholeiitic basaltic rocks (Nb/La > 0.70) from the Baimianshi, Changpu, and Dongkeng basins. Primitive mantle (PM), OIB, E-MORB, and N-MORB compositions are from Sun and McDonough (1989).

6.4. Asthenosphere–metasomatised lithosphere interactions

Most of the basaltic rocks at the base (Unit I and II) of the Yutian Group are the high Nb/La tholeiitic basalts with small Nb—Ta depletions (Figs. 2a and 8), and represent the earliest upwelling of the shallow asthenospheric mantle. At the top of Unit II, minor low Nb/La tholeiitic basalts occur (Figs. 2a and 8), signifying that the beginning of partial melting of the metasomatised lithospheric mantle. Subsequently, the high-Ba tholeiitic basalts with large negative Nb—Ta anomalies are spatially associated with high-Mg andesites–dacites in the lower part of Unit III, suggesting increasing amounts of melts were derived from the metasomatised lithospheric mantle. Moreover, voluminous low Nb/La tholeiitic basalts with moderate Nb—Ta depletions occur in the middle–upper part of Unit III (Figs. 2a and 8). This suggests that the magmas parental to the low Nb/La tholeiitic basalts in Unit III were probably the melts mixing between the parental magmas for the high Nb/La tholeiitic basalts derived from the asthenospheric mantle and for the high-Ba tholeiitic basalts derived from the overlying metasomatised lithospheric mantle.

The occurrence of alkaline basalts (samples ZK3–09 to ZK3–12) with the tholeiitic basalts in the lower–middle part of Unit IV (Figs. 2a and 8) implies the generation of high-Ti alkaline basaltic melts from a deeper asthenospheric mantle source. All the tholeiitic basalts in Unit IV have variable $\varepsilon_{Nd}(t)$ values and Nb—Ta depletions (Figs. 2a and 8), and are also interpreted as the magmas mixing between the parental melts from the asthenospheric and those from the metasomatised lithospheric mantle sources.

There is a temporal progression from the primary low-Ti magmas of the high Nb/La tholeiitic basalts with no obvious Nb—Ta depletions through to the low-Ti melts that were parental to the high-Ba tholeiitic basalts with large negative Nb—Ta anomalies, mixed magmas of the low Nb/La tholeiitic basalts with variable Nb—Ta depletions, and to the high-Ti alkaline basaltic magmas (Figs. 2a and 8). These changes imply initial melting of shallow asthenospheric mantle and the overlying metasomatised lithospheric mantle, and finally propagation of the melting regime into the deeper asthenospheric mantle. Multiple melt sources account for the variable geochemical features of these basalts recovered from drill cores.

6.5. Tectonic implications

The tectonic setting of Jurassic magmatism in inland South China is unclear. Existing models include post-orogenic extension after the Indosinian orogeny (model 1; Wang et al., 2003, 2005; Chen et al., 2008), continental lithospheric extension related to Palaeo-Pacific oceanic plate subduction (model 2; Zhou and Li, 2000; Zhou et al., 2006), back-arc extension associated with slab roll-back of the subducted Palaeo-Pacific oceanic plate (model 3; Jiang et al., 2006, 2009), and continental lithospheric extension in response to the foundering/delamination of a flat-subducted oceanic slab (model 4; Li and Li, 2007). The second and third models suggest that subduction of the Palaeo-Pacific oceanic slab beneath southeastern China did not occur until the Middle Jurassic.

The high Nb/La tholeiitic and alkaline basalts in southern Jiangxi Province were dominantly derived from depleted asthenospheric mantle. Most low Nb/La tholeiitic basalts were generated by melts mixing between the parental magmas for the high Nb/La basalts from the asthenospheric mantle and those for the high-Ba tholeiitic basalts derived from the overlying metasomatised lithospheric mantle (Fig. 11). This explains why the Sr—Nd isotopic compositions of basaltic samples from the Baimianshi, Changpu, and Dongkeng basins are highly variable (Figs. 10–11; Wang et al., 2005; Cen et al., 2016). Previously described basaltic rocks vary from tholeiitic basalts with no obvious Nb—Ta depletions (Wang et al., 2005), to those with moderate–large Nb—Ta depletions (Cen et al., 2016; Fig. 6). Moreover, our new results provide evidence for the presence of a lithospheric mantle metasomatized by

previously subducted oceanic slab beneath southeastern China prior to the Early Jurassic and strong upwelling of the asthenosphere at ca. 190 Ma in inland South China.

Given the temporal–spatial distribution of Triassic–Jurassic igneous rocks described by Li and Li (2007) and the geochemical characteristics of the earliest Jurassic basalts reported in this study, the earliest Jurassic bimodal volcanic rocks in southern Jiangxi Province are unlikely to be related to subduction and closure of the Palaeo-Tethys Ocean, which is >2000 km to the southwest (Metcalfe, 2013). In addition, Liu et al. (2011) and Li et al. (2012) presented evidence that there could have been NNE-trending marginal arc by the normal Palaeo-Pacific subduction in the Early Jurassic (ca. 205–190 Ma). The new continental arc could have triggered slab pull and extension in a back-arc setting. The NNE–SSW-trending Early–Middle Jurassic granite belt in southeastern China (Fig. 1b) is also broadly perpendicular to the NW-ward subduction of the normal Palaeo-Pacific oceanic plate. As such, the formation of the earliest Jurassic bimodal volcanic rocks could have been due to a combined effect of foundering/delamination of a previously subducted Palaeo-Pacific oceanic flat-slab (model 4; Li and Li, 2007) and back-arc extension triggered by steep eastward subduction (Fig. 13).

The 194 Ma Xialan mafic–ultramafic intrusions from northeastern Guangdong have relatively high $\varepsilon_{Nd}(t)$ values (+1.7 to +6.2) and low initial $^{87}Sr/^{86}Sr$ values (0.704–0.706). They also have OIB-like trace element patterns, with slightly negative Nb—Ta anomalies (Zhu et al., 2010). It has been suggested that the Xialan gabbros represent the earliest Jurassic asthenosphere-derived melts. The foundering/delamination of the flat slab can explain the first appearance of both mafic and A-type magmatism in northeastern Guangdong (Gan et al., 2017a, 2017b; Yu et al., 2010; Zhu et al., 2010). Thus, 205–195 Ma (Stage 1; Fig. 13a) magmatism was caused by decompression melting of the upwelling asthenosphere and marks the initiation of slab break-off.

The ca. 190 Ma high Nb/La tholeiitic basalts were generated by partial melting of a depleted asthenospheric mantle source and occur at the base of the volcanic sequence in the Yutian Group (Figs. 2a and 8). Upwelling of asthenospheric mantle led to decompression melting and subsequently induced partial melting of the overlying metasomatised lithospheric mantle, which generated the parental magmas for the high-Ba tholeiitic basalts. From 190 to 155 Ma, this magmatic event formed the widely distributed I- and A-type granites and mafic rocks in inland South China (Fig. 1b–c; Zhou et al., 2006; Li et al., 2007a). Based on the temporal and spatial distribution of these rocks, the 190–155 Ma (Stage 2; Fig. 13b) widespread anorogenic magmatism in southeastern China was triggered by extensive upwelling of asthenospheric mantle. The asthernosphere upwelling may have resulted from the foundering/delamination of the flat slab and back-arc extension caused by the NNE-trending normal Palaeo-Pacific subduction zone in the Early–Middle

Fig. 13

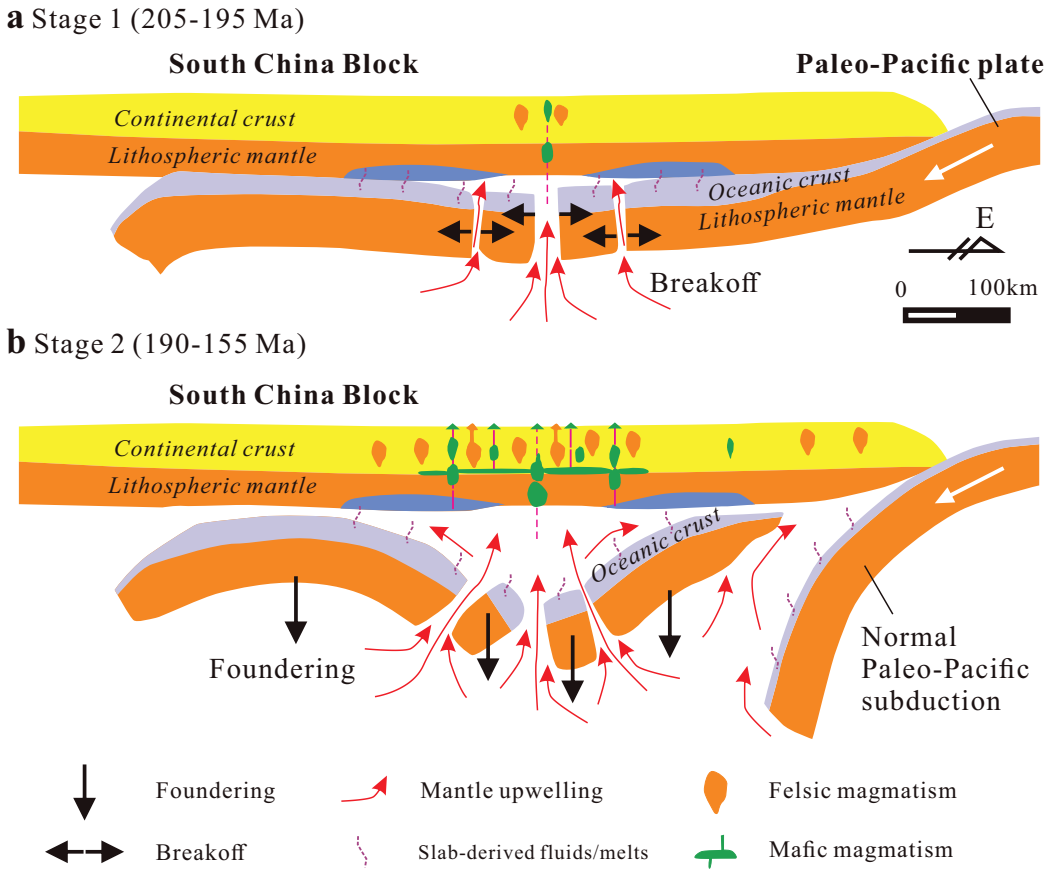

Fig. 13. Schematic geodynamic model for the formation of the (a) Stage 1 (205–195 Ma) mafic–ultramafic intrusions and A-type granites and (b) Stage 2 (190–155 Ma) bimodal volcanic rocks, granites, syenites, and mafic intrusions in southeastern China (modified after Li and Li, 2007; Li et al., 2012).

Jurassic. This model can explain the origins of the widespread Early–Middle Jurassic magmatism in southeastern China.

7. Conclusions

(1) The earliest Jurassic basaltic rocks in the Baimianshi, Changpu, and Dongkeng basins in southern Jiangxi Province consist mainly of tholeiitic basalts and subordinate alkaline basalts. Some of the tholeiitic basaltic rocks are enriched in Ba.
(2) The alkaline basalts show OIB-like trace element characteristics. The trace element compositions of the tholeiitic basalts are intermediate between E-MORBs and IABs. Some of the tholeiitic basalts have trace element compositions similar to E-MORBs, whereas the high-Ba tholeiitic rocks have trace element compositions similar to IABs, such as pronounced negative Nb—Ta anomalies.
(3) It is inferred from the geochemical data that the parental magmas for the high Nb/La tholeiitic basalts and for the alkaline basalts were produced by moderate and low degrees of partial melting of a depleted asthenospheric mantle at the relatively shallow and deep field, respectively. The parental magmas for the high-Ba tholeiitic basaltic rocks were derived from the overlying metasomatised lithospheric mantle. It is suggested that the parental magmas for the low Nb/La tholeiitic basalts with variable Nb—Ta depletions were generated by magma mixing between the parental magmas for the high Nb/La tholeiitic basalts and for the high-Ba tholeiitic basalts.
(4) We suggest propose that the earliest Jurassic basaltic magmatism in the Baimianshi, Changpu, and Dongkeng basins were due to asthenosphere upwelling as a result of delamination/foundering of a the previously subducted flat slab, and a back-arc extensional setting induced by high-angle subduction of the Palaeo-Pacific oceanic plate.

Supplementary data to this article can be found online at https://doi.org/10.1016/j.lithos.2021.106444.

Declaration of Competing Interest

The authors declare that they have no known competing financial interests or personal relationships that could have appeared to influence the work reported in this paper.

Acknowledgements

This research was jointly supported by the National Key Research and Development Program of China (2016YFC0600405) and the National Natural Science Foundation of China (Grants 41572074 and 41273049). We thank X. Chen and S.Y. Guo for their assistance in sampling; B. Wang, J. Hu, Y. Huang and G.P. Bao for their assistance in whole-rock chemical analysis, and N.P. Shen, F. Xiao and J. Wang for their assistance in whole-rock Sr—Nd isotopes analysis. We are grateful that Dr. Chusi Li of Indiana University for his constructive suggestions. The paper also benefited from review comments and suggestions from the editor and two anonymous reviewers.

References

Arndt, N.T., Christensen, U., 1992. The role of lithospheric mantle in continental flood volcanism: thermal and geochemical constraints. J. Geophys. Res. 97, 10967–10981.
Bai, Z.J., Zhu, W.G., Zhong, H., Li, C.S., Liao, J.Q., Sun, H.S., 2015. Petrogenesis and tectonic implications of the early Jurassic Fe–Ti oxide-bearing Xialan mafic intrusion in SE China: Constraints from zircon Hf–O isotopes, mineral compositions and whole-rock geochemistry. Lithos 212–215, 59–73.
Boynton, W.V., 1984. Geochemistry of the rare earth elements: meteorite studies. In: Henderson, P. (Ed.), Rare Earth Element Geochemistry. Elsevier, pp. 63–114.
Brown, J.W., White, R.S., 1995. Effect of finite extension rate on melt generation at rifted continental margins. J. Geophys. Res. Solid Earth 100 (B9), 18011–18029.
Cen, T., Li, W.X., Wang, X.C., Pang, C.J., Li, Z.X., Xing, G.F., Zhao, X.L., Tao, J.H., 2016. Petrogenesis of early Jurassic basalts in southern Jiangxi Province, South China: Implications for the thermal state of the Mesozoic mantle beneath South China. Lithos 256–257, 311–320.
Chen, Z.H., Xing, G.F., 2016. Geochemical and zircon U–Pb–Hf–O isotopic evidence for a coherent Paleoproterozoic basement beneath the Yangtze Block, South China. Precambrian Res. 279, 81–90.
Chen, P.R., Zhou, X.M., Zhang, W.L., Li, H.M., Fan, C.F., Sun, T., Chen, W.F., Zhang, M., 2005. Petrogenesis and significance of early Yanshanian syenite-granite complex in eastern Nanling Range. Sci. China Ser. D Earth Sci. 48, 912–924.
Chen, C., Lee, C., Shinjo, R., 2008. Was there Jurassic paleo–Pacific subduction in South China?: constraints from $^{40}Ar/^{39}Ar$ dating, elemental and Sr–Nd–Pb isotopic geochemistry of the Mesozoic basalts. Lithos 106, 83–92.
Deniel, C., 1998. Geochemical and isotopic (Sr, Nd, Pb) evidence for plume–lithosphere interactions in the genesis of Grande Comore magmas (Indian Ocean). Chem. Geol. 144, 281–303.
Donnelly, K.E., Goldstein, S.L., Langmuir, C.H., Spiegelman, M., 2004. Origin of enriched ocean ridge basalts and implications for mantle dynamics. Earth Planet. Sci. Lett. 226, 347–366.
Gan, C.S., Wang, Y.J., Qian, X., Bi, M.W., He, H.Y., 2017a. Constraints of the Xialan gabbroic intrusion in the Eastern Nanling Range on the early Jurassic intra-continental extension in eastern South China. J. Asian Earth Sci. 145, 576–590.
Gan, C.S., Wang, Y.J., Zhang, Y.Z., Zhang, J., 2017b. The earliest Jurassic A-type granite in the Nanling Range of southeastern South China: petrogenesis and geological implications. Int. Geol. Rev. 59, 274–292.
Garfunkel, Z., 2008. Formation of continental flood volcanism — the perspective of setting of melting. Lithos 100, 49–65.
Gibson, S.A., Kirkpatrick, R.J., Emmerman, R., Schmincke, P.H., Pritchard, G., Okay, P. J., Horpe, R.S., Marriner, G.F., 1982. The trace element composition of the lavas and dykes from a 3 km vertical section through a lava pile of Eastern Iceland. J. Geophys. Res. 87, 6532–6546.
Green, T.H., 1994. Experimental studies of trace-element partitioning applicable to igneous petrogenesis — Sedona 16 years later. Chem. Geol. 117, 1–36.
Hawkesworth, C., Turner, S., McDermott, F., Peate, D., Van Calsteren, P., 1997. U–Th isotopes in arc magmas: implications for element transfer from the subducted crust. Science 276, 551–555.
He, Z.Y., Xu, X.S., 2012. Petrogenesis of the late Yanshanian mantle-derived intrusions in southeastern China: response to the geodynamics of paleo-Pacific plate subduction. Chem. Geol. 328, 208–221.
He, Z.Y., Xu, X.S., Niu, Y.L., 2010. Petrogenesis and tectonic significance of a Mesozoic granite–syenite–gabbro association from inland South China. Lithos 119, 621–641.
Hoernle, K., White, J.D.L., van den Bogaard, P., Hauff, F., Coombs, D.S., Werner, R., Timm, C., Garbe-Schönberg, D., Reay, A., Cooper, A.F., 2006. Cenozoic intraplate volcanism on New Zealand: upwelling induced by lithospheric removal. Earth Planet. Sci. Lett. 248, 350–367.
Jenner, G.A., Longerich, H.P., Jackson, S.E., Fryer, B.J., 1990. ICP-MS—a powerful tool for high precision trace element analyses in earth sciences: evidence from analyses of selected USGS reference samples. Chem. Geol. 83, 133–148.
Ji, C.Y., Wu, J.H., 2010. The SHRIMP zircon U–Pb dating of felsic volcanic rocks and its geological significance from Yutian group in southern Jiangxi. J. East China Institute Technol. 33, 131–138 (in Chinese).
Jiang, Y.H., Jiang, S.Y., Zhao, K.D., Ling, H.F., 2006. Petrogenesis of late Jurassic Qianlishan granites and mafic dykes, Southeast China: implications for a back-arc extension setting. Geol. Mag. 143, 457–474.
Jiang, Y.H., Jiang, S.Y., Dai, B.Z., Liao, S.Y., Zhao, K.D., Ling, H.F., 2009. Middle to late Jurassic felsic and mafic magmatism in southern Hunan province, Southeast China: implications for a continental arc to rifting. Lithos 107, 185–204.
Jiao, S.J., Li, X.H., Huang, H.Q., Deng, X.D., 2015. Metasedimentary melting in the formation of charnockite: Petrological and zircon U-Pb-Hf-O isotope evidence from the Darongshan S-type granitic complex in southern China. Lithos 239, 217–233.
Kepezhinskas, P., Defant, M.J., Drummond, M.S., 1996. Progressive enrichment of island arc mantle by melt–peridotite interaction inferred from Kamchatka xenoliths. Geochim. Cosmochim. Acta 60, 1217–1229.
Kinzler, R.J., 1997. Melting of mantle peridotite at pressures approaching the spinel to garnet transition: application to mid-ocean ridge basalt petrogenesis. J. Geophys. Res. 102, 853–874.
Lassiter, J.C., DePaolo, D.J., 1997. Plume/lithosphere interaction in the generation of continental and oceanic flood basalts: Chemical and isotopic constraints. In: Mahoney, J.J., Coffin, M.F. (Eds.), Large Igneous Province: Continental, Oceanic, and Planetary Flood Volcanism. American Geophysical Union Geophysical Monography, vol. 100, pp. 335–355.
Li, X.H., 2000. Cretaceous magmatism and lithospheric extension in Southeast China. J. Asian Earth Sci. 18, 293–305.
Li, Z.X., Li, X.H., 2007. Formation of the 1300-km-wide intracontinental orogen and postorogenic magmatic province in Mesozoic South China: a flat-slab subduction model. Geology 35, 179–182.
Li, X.H., Sun, M., Wei, G.J., Liu, Y., Lee, C.Y., Malpas, J., 2000. Geochemical and Sm–Nd isotopic study of amphibolites in the Cathaysia Block, southeastern China: evidence for an extremely depleted mantle in the Paleoproterozoic. Precambrian Res. 102, 251–262.
Li, X.H., Li, Z.X., Zhou, H., Liu, Y., Kinny, P.D., 2002. U–Pb zircon geochronology, geochemistry and Nd isotopic study of Neoproterozoic bimodal volcanic rocks in the Kangding Rift of South China: implications for the initial rifting of Rodinia. Precambrian Res. 113, 135–155.

Li, X.H., Chen, Z.G., Liu, D.Y., Li, W.X., 2003. Jurassic Gabbro-Granite-Syenite Suites from Southern Jiangxi Province, SE China: Age, Origin, and Tectonic significance. Int. Geol. Rev. 45, 898–921.
Li, X.H., Chung, S.L., Zhou, H., Lo, C.H., Liu, Y., Chen, C.H., 2004. Jurassic intraplate magmatism in southern Hunan–eastern Guangxi: $^{40}Ar/^{39}Ar$ dating, geochemistry, Sr–Nd isotopes and implications for the tectonic evolution of SE China. Geol. Soc. Lond., Spec. Publ. 226, 193–215.
Li, X.H., Li, W.X., Li, Z.X., 2007a. On the genetic classification and tectonic implications of the early Yanshanian granitoids in the Nanling Range, South China. Chin. Sci. Bull. 52, 1873–1885.
Li, X.H., Li, Z.X., Li, W.X., Liu, Y., Yuan, C., Wei, G., Qi, C., 2007b. U–Pb zircon, geochemical and Sr–Nd–Hf isotopic constraints on age and origin of Jurassic I- and A-type granites from Central Guangdong, SE China: a major igneous event in response to foundering of a subducted flat-slab? Lithos 96, 186–204.
Li, X.H., Li, W.X., Wang, X.C., Li, Q.L., Liu, Y., Tang, G.Q., 2009. Role of mantle-derived magma in genesis of early Yanshanian granites in the Nanling Range, South China: in situ zircon Hf–O isotopic constraints. Sci. China Ser. D Earth Sci. 52, 1262–1278.
Li, Z.X., Li, X.H., Wartho, J.A., Clark, C., Li, W.X., Zhang, C.L., Bao, C., 2010. Magmatic and metamorphic events during the early Paleozoic Wuyi–Yunkai orogeny, southeastern South China: new age constraints and pressure-temperature conditions. Geol. Soc. Am. Bull. 122, 772–793.
Li, Z.X., Li, X.H., Chung, S.L., Lo, C.H., Xu, X.S., Li, W.X., 2012. Magmatic switch-on and switch-off along the South China continental margin since the Permian: transition from an Andean-type to a Western Pacific-type plate boundary. Tectonophysics 532–535, 271–290.
Li, W.X., Li, X.H., Wang, X.C., Yang, D.S., 2017. Petrogenesis of cretaceous shoshonitic rocks in the northern Wuyi Mountains, South China: a result of the roll-back of a flat-slab? Lithos 288–289, 125–142.
Liu, Q., Yu, J.H., Su, B., Wang, Q., Tang, H.F., Xu, H., Cui, X., 2011. Discovery of the 187 Ma granite in Jincheng area, Fujian Province: Constraint on early Jurassic tectonic evolution of southeastern China. Acta Petrol. Sin. 27, 3575–3589.
McKenzie, D.P., O'Nions, R.K., 1991. Partial melt distribution from inversion of rare earth element concentrations. J. Petrol. 32, 1021–1991.
McKenzie, D.P., O'Nions, R.K., 1995. The source regions of ocean island basalts. J. Petrol. 36, 133–159.
Meng, L.F., Li, Z.X., Chen, H.L., Li, X.H., Wang, X.C., 2012. Geochronological and geochemical results from Mesozoic basalts in southern South China Block support the flat-slab subduction model. Lithos 132–133, 127–140.
Metcalfe, I., 2013. Gondwana dispersion and Asian accretion: tectonic and palaeogeographic evolution of eastern Tethys. J. Asian Earth Sci. 66, 1–33.
Miyashiro, A., 1974. Volcanic rock series in island arcs and active continental margins. Am. J. Sci. 274, 321–355.
Pik, R., Deniel, C., Coulon, C., Yirgu, G., Marty, B., 1999. Isotopic and trace element signatures of Ethiopian flood basalts: evidence for plume–lithosphere interaction. Geochim. Cosmochim. Acta 63, 2263–2279.
Qi, L., Hu, J., Gregoire, D.C., 2000. Determination of trace elements in granites by inductively coupled plasma mass spectrometry. Talanta 51, 507–513.
Qi, C.S., Deng, X.G., Li, W.X., Li, X.H., Yang, Y.H., Xie, L.W., 2007. Origin of the Darongshan-Shiwandashan S-type ganiteoid belt from southeastern Guangxi: geochemical and Sr-Nd-Hf isotopic constraints. Acta Petrol. Sin. 23, 403–412.
Rudnick, R.L., Fountain, D.M., 1995. Nature and composition of the continental crust: a lower crustal perspective. Rev. Geophys. 33, 267–309.
Saunders, A.D., 2005. Large igneous provinces: origin and environmental consequences. Elements 1, 259–263.
Shaw, D.M., 1970. Trace element fractionation during anatexis. Geochim. Cosmochim. Acta 34, 237–243.
Stewart, K., Rogers, N., 1996. Mantle plume and lithosphere contributions to basalts from southern Ethiopia. Earth Planet. Sci. Lett. 139, 195–211.
Sun, S.S., McDonough, W.F., 1989. Chemical and isotopic systematics of oceanic basalts: Implications for mantle composition and processes. In: Saunders, A.D., Norry, M.J. (Eds.), Magmatism in the Ocean Basins, vol. 42. Geological Society, London Special Publications, pp. 313–345.
Tang, G.J., Wang, Q., Wyman, D.A., Li, Z.X., Xu, Y.G., Zhao, Z.H., 2012. Metasomatized lithosphere–asthenosphere interaction during slab roll-back: evidence from late Carboniferous gabbros in the Luotuogou area, Central Tianshan. Lithos 155, 67–80.
Tatsumi, Y., Eggins, S., 1995. Subduction Zone Magmatism. Blackwell, Cambridge, p. 211.
Timm, C., Hoernle, K., Van Den Bogaard, P., Bindeman, I., Weaver, S., 2009. Geochemical evolution of intraplate volcanism at Banks Peninsula, New Zealand: interaction between asthenospheric and lithospheric melts. J. Petrol. 50, 989–1023.
Walter, M.J., 1998. Melting of garnet peridotite and the origin of komatiite and depleted lithosphere. J. Petrol. 39, 29–60.
Wan, Y.S., Liu, D.Y., Wilde, S.A., Cao, J.J., Chen, B., Dong, C.Y., Song, B., Du, L.L., 2010. Evolution of the Yunkai Terrane, South China: evidence from SHRIMP zircon U–Pb dating, geochemistry and Nd isotope. J. Asian Earth Sci. 37, 140–153.
Wang, Y.J., Fan, W.M., Guo, F., Peng, T.P., Li, C.W., 2003. Geochemistry of Mesozoic mafic rocks adjacent to the Chenzhou-Linwu fault, South China: implications for the lithospheric boundary between the Yangtze and Cathaysia Blocks. Int. Geol. Rev. 45, 263–286.
Wang, Y.J., Fan, W.M., Peng, T.P., Guo, F., 2005. Elemental and Sr–Nd isotopic systematics of the early Mesozoic volcanic sequence in southern Jiangxi Province, South China: petrogenesis and tectonic implications. Int. J. Earth Sci. 94, 53–65.
Wang, Y.J., Fan, W.M., Cawood, P.A., Li, S.Z., 2008. Sr–Nd–Pb isotopic constraints on multiple mantle domains for Mesozoic mafic rocks beneath the South China Block hinterland. Lithos 106, 297–308.
White, R., McKenzie, D., 1989. Magmatism at rift zones: the generation of volcanic continental margins and flood basalts. J. Geophys. Res. 94 (B6), 7685–7729.
Winchester, J.A., Floyd, P.A., 1976. Geochemical magma type discrimination: application to altered and metamorphosed basic igneous rocks. Earth Planet. Sci. Lett. 28, 459–469.
Wood, D.A., Joron, J.L., Treuil, M., 1979. A re-appraisal of the use of trace elements to classify and discriminate between magma series erupted in different tectonic settings. Earth Planet. Sci. Lett. 45, 326–336.
Wu, J.H., Zhou, W.X., Zhang, B.T., 2000. Stratigraphic division and geologic era of Mesozoic era volcanic rock series in South Jiangxi–North Guangdong. Geol. Rev. 46, 362–370 (in Chinese).
Xie, X., Xu, X.S., Zou, H.B., Jiang, S.Y., Zhang, M., Qiu, J.S., 2006. Early J_2 basalts in SE China: incipience of large-scale late Mesozoic magmatism. Sci. China Ser. D Earth Sci. 49, 796–815.
Yu, J.S., Gui, X.T., Yuan, C., 1999. The characteristics of isotopes geochemistry of darongshan granitoid suite, Guangxi. Guangxi Geol. 12, 1–6 (in Chinese).
Yu, J.H., Wang, L.J., Griffin, W.L., O'Reilly, S.Y., Zhang, M., Li, C.-Z., Shu, L.S., 2009. A Paleoproterozoic orogeny recorded in a long-lived cratonic remnant (Wuyishan terrane), eastern Cathaysia Block, China. Precambrian Res. 174, 347–363.
Yu, X.Q., Wu, G.G., Zhao, X., Gao, J.F., Di, Y.J., Zheng, Y., Dai, Y.P., Li, C.L., Qiu, J.T., 2010. The early Jurassic tectono-magmatic events in southern Jiangxi and northern Guangdong provinces, SE China: constraints from the SHRIMP zircon U–Pb dating. J. Asian Earth Sci. 39, 408–422.
Zhang, B.T., Chen, P.R., Kong, X.G., 2002. Rb-Sr chronology of bimodal volcanic rocks of the Yutian Group in the Linjiang basion, southern Jiangxi. Geol. China 29, 352–354 (in Chinese).
Zhou, X.M., Li, W.X., 2000. Origin of late Mesozoic igneous rocks in Southeastern China: implications for lithosphere subduction and underplating of mafic magmas. Tectonophysics 326, 269–287.
Zhou, J.C., Jiang, S.Y., Wang, X.L., Yang, J.H., Zhang, M.Q., 2005. Re–Os isochron age of Fankeng basalts from Fujian of SE China and its geological significance. Geochem. J. 39, 497–502.
Zhou, X.M., Sun, T., Shen, W.Z., Shu, L.S., Niu, Y.L., 2006. Petrogenesis of Mesozoic granitoids and volcanic rocks in South China: a response to tectonic evolution. Episodes 29, 26–33.
Zhu, W.G., Zhong, H., Li, X.H., He, D.F., Song, X.Y., Ren, T., Chen, Z.Q., Sun, H.S., Liao, J. Q., 2010. The early Jurassic mafic–ultramafic intrusion and A-type granite from northeastern Guangdong, SE China: Age, origin, and tectonic significance. Lithos 119, 313–329.
Zhu, W.G., Zhong, H., Chen, X., Huang, H.Q., Bai, Z.J., Yao, J.H., Wang, Y.J., Hu, P.C., 2020. The earliest Jurassic A-type rhyolites and high-Mg andesites–dacites in southern Jiangxi Province, Southeast China: evidence for delamination of a flat-slab? Lithos 358–359, 105403.